Precambrian Research 389 (2023) 107002

Contents lists available at ScienceDirect

Precambrian Research

journal homepage: www.elsevier.com/locate/precamres

Proterozoic evolution of the Alxa block in western China: A wandering terrane during supercontinent cycles

Wenhao Su [a], Qin Wang [a,*], Jian Kang [b], Xieyan Song [b]

[a] State Key Laboratory for Mineral Deposits Research, School of Earth Sciences and Engineering, Nanjing University, Nanjing, China
[b] State Key Laboratory of Ore Deposit Geochemistry, Institute of Geochemistry, Chinese Academy of Sciences, Guiyang 550081, China

ARTICLE INFO

Keywords:
Alxa block
Zircon U-Pb age
Hf isotope
North China craton
Yangtze craton
Supercontinent

ABSTRACT

The tectonic affinity of the Alxa block in the western North China craton remains controversial because of the widespread Cenozoic sediments and limited Proterozoic geochronological data, especially in the western Alxa block. To establish the tectonic affinity of the Alxa block with neighbor units, we systematically investigated U-Pb age and Hf isotope composition of zircon and U-Th-Pb age of monazite from Proterozoic rocks in the southwestern Alxa block. Ages of zircon and monazite from granitic gneiss and mica schist indicate that the Paleoproterozoic Longshoushan Complex recorded a magmatic event at ~2.0 Ga and two metamorphic events at ~1.95–1.90 and ~1.85–1.80 Ga. Detrital zircons from quartz schist of the Longshoushan Complex show an age peak at ~2.0 Ga with εHf(t) values between −4.048 and 6.432. By contrast, detrital zircons from the Late Paleoproterozoic Dunzigou Group yield different Paleoproterozoic age peaks and εHf(t) values, suggesting a provenance change. Detrital zircons from the Neoproterozoic Hanmushan Group exhibit three age peaks at ~2.5 Ga, ~1.85 Ga and ~0.8 Ga, and two types of εHf(t) values with wide variations. The depositional ages of the Dunzigou Group and Hanmushan Group are constrained as 1.8–1.7 Ga and 845–830 Ma, respectively. The detrital zircon age populations suggest that the Longshoushan area experienced a transition from a convergent setting (less polymodal age spectra) at ~1.98–1.95 Ga to a divergent setting (polymodal age spectra) at 1.8–1.7 Ga and then intracontinental rifting at ~830 Ma. Compared with previous zircon studies, we propose that the Alxa block may be connected with the Khondalite belt at ~1.98–1.90 Ga during assemblage of the Columbia supercontinent, and located between the North China craton and the northern Siberian craton at 1.8–1.7 Ga in a divergent setting. The Alxa block probably separated from the North China craton in the Late Mesoproterozoic and moved next to the northwestern Yangtze craton in the Early Neoproterozoic during the assemblage and breakup of the Rodinia supercontinent.

1. Introduction

The tectonic framework of China is characterized by the amalgamation of multiple Precambrian blocks along collisional belts (Fig. 1a) (e.g., Zhao and Cawood, 2012; Yang et al., 2016; Li et al., 2018a). Extensive studies have been carried out on the formation and evolution of three major cratons, i.e., the North China craton (NCC), the Yangtze craton, and the Tarim craton (e.g., Zhao et al., 2005; Kusky, 2011; Zhai and Santosh, 2011; Zhao and Cawood, 2012). The NCC experienced the collision of the Eastern Block and the Western Block along the Trans-North China orogen at 1.85 Ga (Zhao et al., 2001) or 2.5 Ga (Li et al., 2000; Kusky and Li, 2003). The South China block was formed by the assemblage of the Yangtze craton and the Cathaysia block along the Jiangnan orogen in the Neoproterozoic (Li et al., 2009; Zhao and Cawood, 2012; Cawood et al., 2018; Yao et al., 2019; etc.). However, the affinity and position of these cratons relative to the Columbia and Rodinia supercontinents are still under debate (Zhao et al., 2002; Zhai et al., 2003; Zhai and Santosh, 2011; Zhang et al., 2012; Zhao et al., 2018a; Cawood et al., 2018, 2020).

Microcontinent blocks play an important role in plate reconstruction and the growth history of the continental crust (Li et al., 2018a, b). The Alxa block is located in the western NCC and to the north of the North Qilian orogenic belt, leading to its potential affinity with surrounding tectonic units (Fig. 1). Different models have been proposed for the Precambrian evolution of the Alxa block: (1) The Alxa block was the western extension of the Yinshan block (Zhao et al., 2005; Zhao, 2009),

* Correspondent author.
E-mail address: qwang@nju.edu.cn (Q. Wang).

https://doi.org/10.1016/j.precamres.2023.107002
Received 20 September 2022; Received in revised form 21 December 2022; Accepted 14 February 2023
Available online 24 March 2023

and the Tarim-Dunhuang-Yinshan blocks may be a coherent continental landmass during the Neoarchean to Early Paleoproterozoic period (Ge et al., 2013); (2) the Alxa block was the western extension of the Khondalite belt (Dong et al., 2007; Geng et al., 2010; Zhang et al., 2013b; Gong et al., 2016; Zhang and Gong, 2018); (3) the Alxa block had a stronger affinity to the South China block during the Neoproterozoic in the Rodinia supercontinent (Li et al., 2005; Song et al., 2017).

The Longshoushan ("shan" means mountain in Chinese) at the southwestern margin of the Alxa block is characterized by the well-preserved Paleoproterozoic basement (the Longshoushan Complex) and overlying Proterozoic sequences (the Dunzigou Group and the Hanmushan Group). The ~825 Ma Jinchuan ultramafic intrusion in Longshoushan formed the third largest Cu-Ni-Platinum-group elements sulfide deposit in the world, which has been related with the mantle plume in the South China block (Li et al., 2005; Song et al., 2012; Porter, 2016 and references therein). Recent studies of detrital zircon ages from the Proterozoic rocks in the Longshoushan area proposed its affinity to the Qilian orogenic belt (Wu et al., 2021) or to the South China block (Song et al., 2017). Because global geological events such as supercontinent assemblage and breakup can produce detrital zircons from different source areas with the same age, it is necessary to use zircon Hf isotope composition for the provenance analysis (e.g., Scherer et al., 2007; Wu et al., 2007).

To better constrain the tectonic affinity and position of the Alxa block in the Columbia and Rodinia supercontinents, we measured U-Pb ages and Hf isotope of zircon and U-Th-Pb ages of monazite from the Paleoproterozoic to Neoproterozoic rocks in the Longshoushan area. The results provide new constraints on age and provenance of Proterozoic rocks in the Longshoushan area, which allow us to discuss the tectonic evolution of the Alxa block during supercontinent cycles.

2. Geological background

The triangular-shaped Alxa block in the westernmost NCC is bounded by the Longshoushan fault from the North Qilian orogenic belt in the south, and connected with the Tarim craton along the Altyn Tagh fault in the west (Fig. 1b). The northern Alxa area was involved in the Central Asian orogenic belt and has ophiolite mélanges exposed along two fault belts. Because the western extension of the two fault belts is covered by Badain Jaran Desert, the closure process of the Paleo-Asian Ocean is still under debate. The boundary between the Alxa block and the Central Asian orogenic belt was defined as the Engeerwusu fault (Feng et al., 2013; Zheng et al., 2014; Zhang et al., 2015a), or the Badain Jaran fault (Zhang et al., 2015b; Zheng et al., 2018; Zhang and Gong, 2018). To the east, the NNE-trending Bayanwulashan-Langshan fault separates the Alxa block from the Ordos block in the NCC (Zhang et al., 2015a; Song et al., 2017).

Covered by the widespread Cenozoic sediments, the basement of the Alxa block is mainly exposed in the northeastern and southwestern areas. The Diebusige Complex and the Bayanwulashan Complex in the northeastern Alxa block were formed at ~ 2.3 Ga and experienced two metamorphic events at ~ 1.9 Ga and ~ 1.8 Ga (Dan et al., 2012a; Wu et al., 2014). Dan et al. (2012a) found that the rock assemblages in the northeastern Alxa block are different from the ~ 2.5 Ga tonalitic-trondhjemitic-granodioritic (TTG) rocks in the Yinshan block, and the Yinshan block does not contain rocks as old as ~ 2.34–2.30 Ga or metamorphosed at ~ 1.8 Ga. On the other hand, magmatic and metamorphic zircons from the basement rocks of the Alxa block and the Khondalite belt show similar U-Pb ages, and zircon Lu-Hf data also suggest the coeval crustal growth in the two units during the Neoarchean and Paleoproterozoic (Gong et al., 2012; Zhang et al., 2013b; Gong et al., 2016; Zeng et al., 2018). Therefore, the Alxa block is

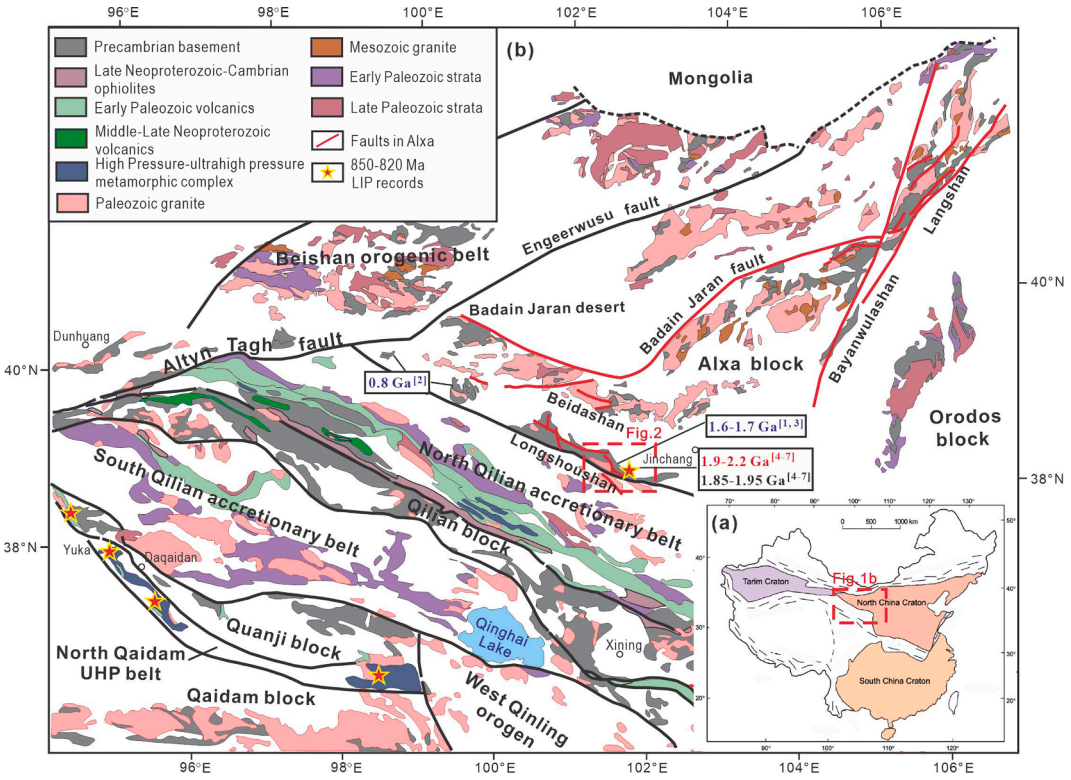

Fig. 1. (a) Tectonic framework of China (Zhao and Cawood, 2012). (b) Simplified geological map of the Alxa block and adjacent regions [modified after Li et al. (2020) and Song et al. (2017)]. Red stars show ~ 850–820 Ma mantle plume records in Jinchuan (Li et al., 2005) and the North Qaidam ultrahigh-pressure (UHP) belt (Xu et al., 2016 and references therein). Zircon ages from previous studies are shown in blue for the maximum depositional age ([1] Song et al., 2017; [2] Tung et al., 2007a; [3] Wu et al., 2021), red for crystallization age and black for metamorphic age ([4] Yan et al., 2015; [5] Gong et al., 2016; [6] Zeng et al., 2018; [7] Wu et al., 2021).

generally regarded as a part of the Khondalite belt during the Neoarchean-Paleoproterozoic.

In the southwestern Alxa block, the Beidashan Complex contains ~ 2.5 Ga granitic gneiss and was subjected to metamorphism at ~ 1.85 Ga (Gong et al., 2012; Zhang et al., 2013b). To the south, the Longshoushan area is a NWW-trending belt of ~ 500 km long and 30 km wide with Proterozoic outcrops (Fig. 1b). As shown in Figs. 2-3, the Paleoproterozoic Longshoushan Complex is mainly composed of foliated granitic gneiss, amphibolite, marble and mica schist, which was intruded by the ~ 825 Ma Jinchuan ultramafic intrusion (Li et al., 2005; Yang et al., 2005; Yang et al., 2008; Zhang et al., 2010). The Longshoushan Complex recorded prolonged magmatism with a peak at ~ 2.1–2.0 Ga and metamorphism at 1.95–1.8 Ga (Xiu et al., 2004; Yan et al., 2015a; Gong et al., 2016; Zeng et al., 2018). The Dunzigou Group consists of foliated carbonate rocks, quartzite and schist and overlies the Longshoushan Complex along a regional unconformity (Gong et al., 2011, 2016). The Dunzigou Group is generally regarded as Mesoproterozoic because of the whole-rock Rb-Sr isochron age of 1261 ± 21 Ma (Li, 1991). An angular unconformity separates the Dunzigou Group from the overlying Neoproterozoic Hanmushan Group, which is mainly composed of siliciclastic rocks, limestone, phyllite and schist. So far the depositional ages of the Dunzigou and Hanmushan groups have not been well constrained by zircon geochronology.

Recent studies of detrital zircon ages in the Longshoushan area raised questions about the tectonic affinity of the Alxa block in the Proterozoic. Detrital zircon age patterns from metasedimentary rocks in the Longshoushan Complex (Gong et al., 2016) and in the Dunzigou Group (Wu et al., 2021) suggest that the Alxa block was an integrated part of the NCC during the Paleoproterozoic and Mesoproterozoic. However, detrital zircons from the Neoproterozoic metasedimentary rocks in the westernmost Longshoushan area is characterized by a peak at the Meso-Neoproterozoic, implying an affinity of the western Longshoushan with the South China block during the Neoproterozoic (Song et al., 2017). Xiao et al. (2019) argued that the Alxa block was not close to the South China block in the Neoproterozoic because the U-Pb age peaks and εHf (t) of zircons of the Alxa block are not similar to the coeval zircons in the Yangtze craton. Wu et al. (2021) pointed out that the age pattern of the Neoproterozoic metasedimentary rocks in Song et al. (2017) is comparable to the coeval sedimentary rocks in the Qilian orogenic belt (Gehrels et al., 2003; Tung et al., 2007b).

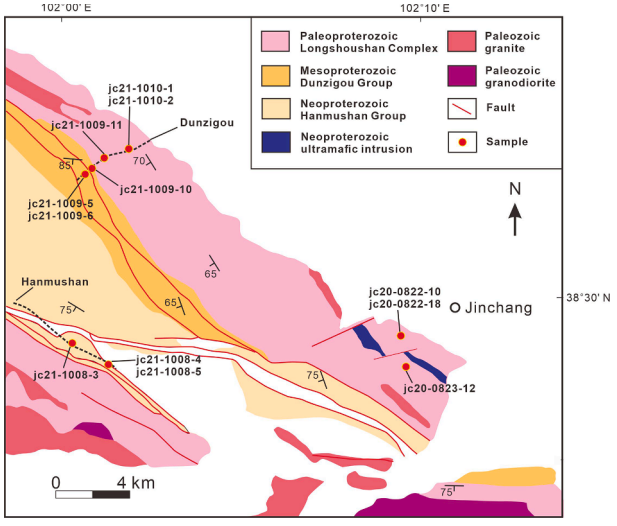

Fig. 2. Simplified geological map of the Jinchang area and sample location (modified after BGGP, 1967).

3. Sample description

We collected 12 samples from the middle Longshoushan area near Jinchang city, including granitic gneiss and quartz schist from the Longshoushan Complex and (meta)sedimentary rocks from the Dunzigou Group and the Hanmushan Group (Figs. 2-3). The sample locality, GPS data, modal composition and dating results are summarized in Supplementary Table S1.

Granitic gneiss samples of the Longshoushan Complex were collected in the mining area of the Jinchuan ultramafic intrusion (Fig. 2). Granitic gneiss samples jc20-0822–10 and jc20-0822–18 were deformed with well-developed foliation (Fig. 4a-b). They have similar modal composition with K-feldspar (42–50%), quartz (~33–40 %), muscovite (12–15%) and minor accessory minerals. Migmatite sample jc20-0823–12 experienced partial melting (Fig. 4c) and consists of quartz (~42%), feldspar (~40%), biotite (~11%), chlorite (~3%) and minor accessory minerals. The three samples represent the county rocks of the Jinchuan mafic–ultramafic intrusion, and show grain boundary migration of quartz in thin sections (Fig. 5a).

Samples in the Dunzigou area were collected along a valley (Fig. 2). Foliated garnet-bearing mica schist samples jc21-1010–1 and jc21-1010–2 belong to the Longshoushan Complex (Fig. 4d and Fig. 5b). They are mainly composed of quartz, feldspar, biotite and muscovite, with minor chlorite and garnet (Table S1). Weakly deformed quartz schist sample jc21-1009–11 (Fig. 4e) shows undulose extinction and grain boundary migration of quartz in thin section (Fig. 5c). Metasedimentary rocks of the Dunzigou Group are strongly deformed. Sheared gravels in conglomerate at the bottom of the Dunzigou Group distribute along the foliation (Fig. 4f). Quartzite sample jc21-1009–10 was collected from the conglomerate layer (Fig. 5d). Quartz schist sample jc21-1009–6 (Fig. 4g) and quartzite sample jc21-1009–5 (Fig. 4h) show clear foliation, mainly composed of quartz and muscovite. Undulose extinction and bulging recrystallization of quartz in quartz schist and quartzite samples from the Dunzigou Group (Fig. 5) suggest ductile deformation under low-grade metamorphic conditions.

Three (meta)sedimentary rock samples of the Hanmushan Group were collected from the Hanmushan area, about 12 km to the southwest of Jinchang city (Fig. 2). Steeply dipping brownish sandstone sample jc21-1008–5 overlies grey-white sandstone sample jc21-1008–4 (Fig. 4i), both predominantly composed of quartz (Fig. 5e). Metasandstone sample jc21-1008–3 (Fig. 4j) consists of calcite (55%) and quartz (45%), showing dynamic crystallization of quartz (Fig. 5f).

4. Methods

Three granitic gneiss samples and seven (meta)sedimentary samples were selected for zircon U-Pb-Hf analysis, and two mica schist samples were selected for monazite U-Th-Pb analysis. Zircon and monazite grains were separated from crashed samples by density and magnetic techniques. The TESCAN MIRA3 Field Emission Scanning Electron Microscope was used for cathodoluminescence (CL) and backscattered electron (BSE) imaging at Nanjing Hongchuang Geological Exploration Technology Service Company Ltd. The CL and BSE images were used to investigate the internal structure of zircon and monazite.

Zircon U-Pb dating of granitic gneiss samples (jc20-0822–10, jc20-0822–18, and jc20-0823–12) were performed by LA-ICP-MS at the State Key Laboratory of Ore Deposit Geochemistry, Institute of Geochemistry, Chinese Academy of Sciences, Guiyang, China. Agilent 7900 ICP-MS is equipped with a GeoLasPro 193 nm ArF excimer laser, using a laser repetition of 5 Hz and spot size of 32/24 μm. We analyzed two 91,500 samples (Wiedenbeck et al., 1995), a Plešovice sample (Sláma et al., 2008) and a Qinghu sample (Li et al., 2013) after the analysis of every fifteen zircon spots to observe the state and repeatability of the instrument.

The other experiments on zircon and monazite were performed at the State Key Laboratory for Mineral Deposits Research, Nanjing University.

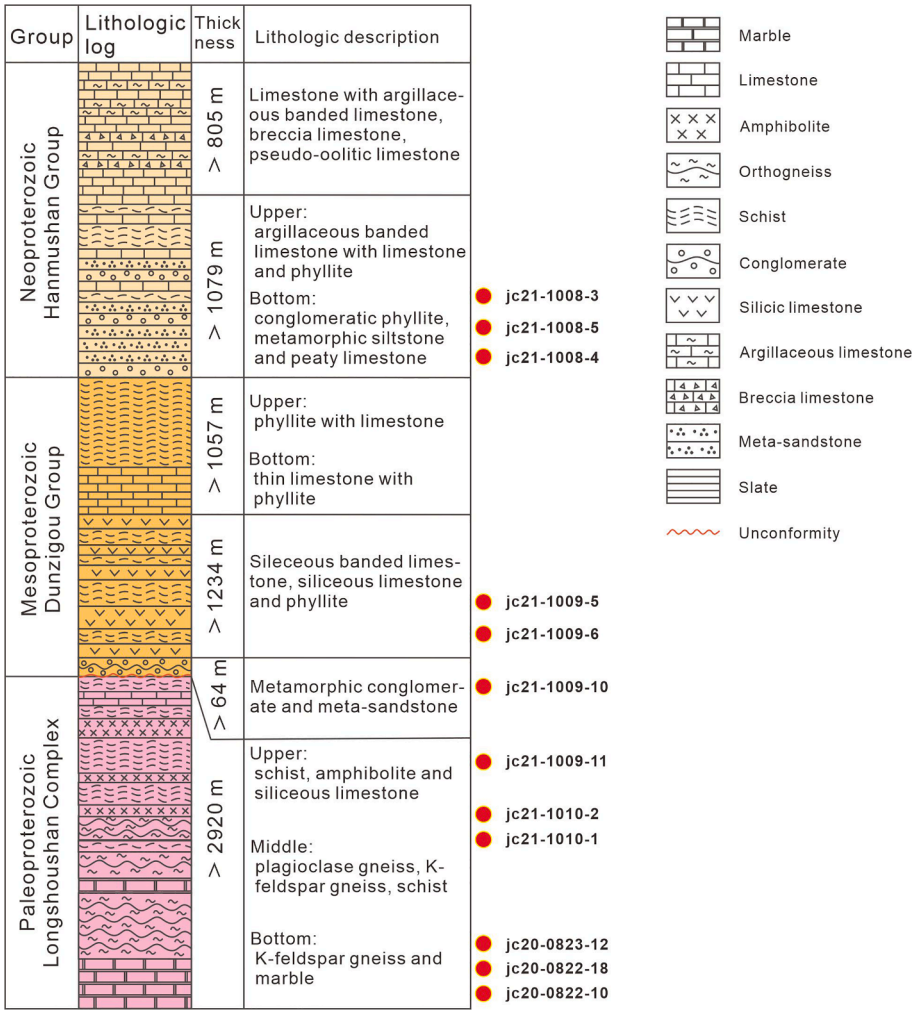

Fig. 3. Stratigraphic column of the Proterozoic strata in the Longshoushan area (modified after Liu et al., 2020b).

Zircon U-Pb dating for the other samples was analyzed by LA-ICP-MS using a Thermo iCAPQ quadrupole ICP-MS attached to a Geolas 213-nm laser ablation system. This equipment was also used for monazite U-Th-Pb dating. Helium was used as carrier gas. For zircon dating, the spot size and laser frequency were 29 μm and 5 Hz, respectively. For every fifteen zircon spots, the U-Pb fractionation was corrected by two 91,500 samples (Wiedenbeck et al., 1995), and the accuracy was controlled by one Plešovice sample (Sláma et al., 2008). The concentrations of trace elements in both labs were calibrated using ^{29}Si as an internal standard and NIST SRM610 and NIST SRM612 as the reference standard. The isotopic ratios and U-Pb age were calculated using ICP-MSDataCal software (Liu et al., 2010). The age calculations and diagrams were made using the ISOPLOT/Ex program (Version 4) (Ludwig, 2012). Zircon U-Pb isotopic compositions are listed in Supplementary Table S2. The errors in the isotope ratios and single grain ages are given at 1σ.

Lu-Hf isotope analyses for zircon were performed following U-Pb analyses using a Thermo Finnigan Neptune-plus MC-ICP-MS fitted with an ArF excimer laser ablation system. Lu-Hf isotopic compositions were analyzed for zircon near the same sites where U-Pb analyses were carried out. A laser repetition of 8 Hz and a spot size of 44 μm were used for this study. The isobaric interference and instrumental mass bias correction followed the method of Chu et al. (2002) and Wu et al. (2006). Zircon 91,500 and TEMORA were used as the reference standard and gave a mean average $^{176}Lu/^{177}Hf$ ratio of 0.282298 ± 0.000010 (2σ, n = 19) and 0.282693 ± 0.000004 (2σ, n = 42), respectively, indistinguishable from the ratio of 0.282307 ± 0.000031 and 0.282680 ± 0.000031 by solution analysis method (Wu et al., 2006). The decay constant of 1.867×10^{-11} $year^{-1}$ for ^{176}Lu (Scherer et al., 2001) and the present-day chondritic values of $^{176}Lu/^{177}Hf$ (0.0332) and $^{176}Hf/^{177}Hf$ (0.282772) (Blichert-Toft and Albarède, 1997) were adopted to calculate the initial values of $^{176}Hf/^{177}Hf$ and εHf (t). Depleted mantle Hf model ages (T_{DM}^{C}) were calculated from the measured $^{176}Lu/^{177}Hf$ and $^{176}Hf/^{177}Hf$ ratios of the zircons, assuming a present-day $^{176}Hf/^{177}Hf$ ratio of 0.283250 and a $^{176}Lu/^{177}Hf$ ratio of 0.0384 for the depleted mantle (Griffin et al., 2002). The average crustal $^{176}Lu/^{177}Hf$ value of 0.015 was adopted to calculate the two-stage Hf model ages (T_{DM}^{C}) (Griffin et al., 2002). The Lu-Hf isotopic data of zircon in this study are listed in Supplementary Table S3.

For monazite U-Th-Pb dating, the spot size and laser frequency were 19 μm and 3 Hz, respectively. For every eight monazite spots, the U-Pb fractionation was corrected by two 117531 samples, and the accuracy was controlled by one KT-252 sample. The calibration method for trace element concentrations in monazite is the same as for zircon. More details are described by Hu et al. (2020). The detailed results for monazite are presented in Supplementary Table S4. The errors in the isotope ratios and single grain ages are given at 1σ.

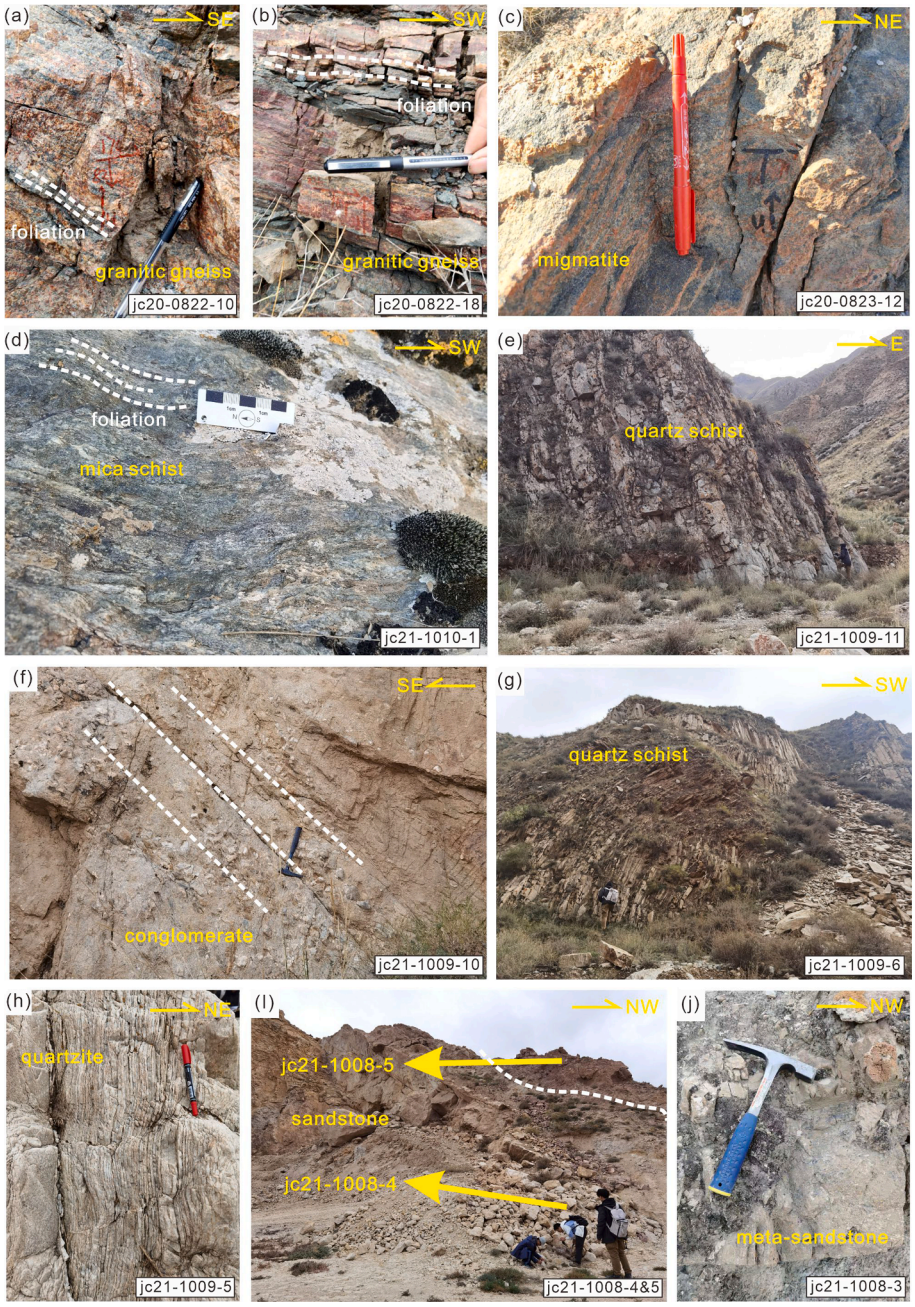

Fig. 4. Field photographs of typical samples in the Longshoushan area. (a-b) Granitic gneiss and (c) migmatite in the Jinchang mining area; (d) Foliated garnet-bearing mica schist and (e) weakly deformed quartz schist from the Longshoushan Complex; (f) Conglomerate with aligned gravels, (g) folded quartz schist and (h) sheared quartzite from the Dunzigou Group; (i) Brownish sandstone and grey-white sandstone, and (j) *meta*-sandstone from the Hanmushan Group near the Hanmu temple.

5. Results

5.1. Zircon U-Pb ages

Individual zircon ages in the following sections were reported with uncertainties at 1σ level. $^{207}Pb/^{206}Pb$ ages were used for zircons older than 1000 Ma, and $^{206}Pb/^{238}U$ ages for zircons younger than 1000 Ma. For (meta)sedimentary rocks, the zircon ages with the discordant < 10% are selected. The Th/U ratios of detrital zircons from our samples are generally > 0.1, indicating a magmatic origin. Zircon grains with the Th/U ratio < 0.1 are not included in U-Pb concordia diagrams and Kernel Density Estimate and histograms.

5.1.1. Ages of the Longshoushan Complex

In CL images, zircons separated from granitic gneiss samples jc20-0822–10 and jc20-0822–18 are subhedral to anhedral. Prismatic to sub-rounded zircon crystals are ~ 100–200 μm in length with a length/width ratio of approximately 1:1 to 3:1 (Fig. 6a). Most zircons show homogeneous texture with weak or no oscillatory features. Relatively low Th/U ratios of 0.008–0.107 (Supplementary Table S2) suggest that these zircons are typical metamorphic zircons. A few zircon grains have the core-rim structure with a relatively strong luminescent core, suggesting a magmatic origin of the cores (Fig. 6a). A bright thin rim is observed in some grains as evidence of a later tectono-thermal event, but it is too thin to date. U-Pb ages of magmatic zircon cores yield the crystallization ages of granite, whereas those of metamorphic zircons constrain the

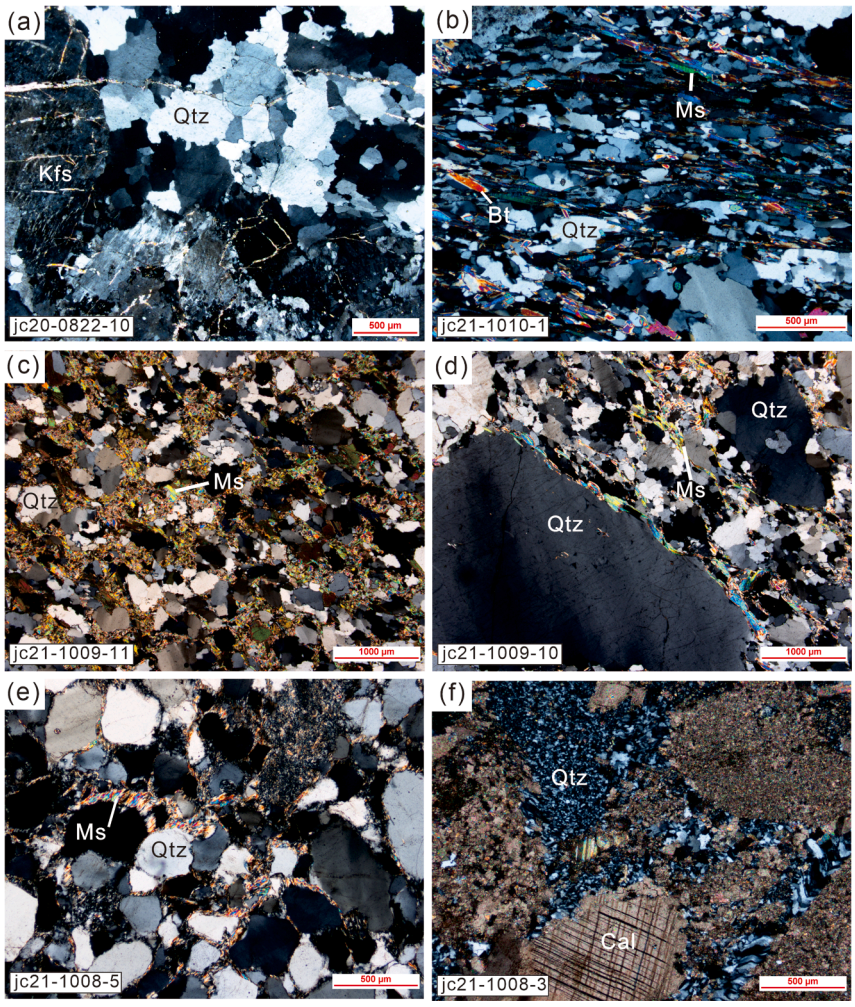

Fig. 5. Photomicrographs of typical Proterozoic samples in the Longshoushan area. (a) Coarse-grained K-feldspar and grain boundary migration of quartz in granitic gneiss; (b) Foliation defined by stretched of quartz and muscovite in garnet-bearing mica schist; (c) Weakly deformed quartz schist; (d) Coarse-grained porphyroclasts and fine-grained dynamically recrystallized quartz from sheared quartzite gravel; (e) Sandstone and (f) coarse-grained calcite-bearing metasandstone. Abbreviations: Qtz-quartz, Kfs-K-feldspar, Bt-biotite, Ms-muscovite, Cal-calcite.

timing of zircon growth during high-grade metamorphism in the Longshoushan Complex.

For sample jc20-0822–10, 66 spots on metamorphic zircons yield $^{207}Pb/^{206}Pb$ ages from 1758 to 1920 Ma, which constrain an upper intercept age of 1844 ± 10 Ma (MSWD = 1.01) (Fig. 7a). A weighted mean $^{207}Pb/^{206}Pb$ age of 1835 ± 12 Ma (MSWD = 1.18) is interpreted as the timing of high-grade metamorphism. Thirty-seven spots on metamorphic zircons from sample jc20-0822–18 show $^{207}Pb/^{206}Pb$ ages from 1736 to 1876 Ma. A discordia trend defines an upper intercept age of 1838 ± 14 Ma (MSWD = 0.43) (Fig. 7b), which agrees with the weighted mean $^{207}Pb/^{206}Pb$ age of 1810 ± 16 Ma (MSWD = 0.43). For the two samples, only three spots on magmatic cores were dated with the $^{207}Pb/^{206}Pb$ age of 2009 ± 43 Ma, 2072 ± 46 Ma, and 2035 ± 50 Ma, older than their metamorphic ages.

Zircons from migmatite sample jc20-0823–12 show similar features with the two granitic gneiss samples. Among 88 spots on zircon grains, 67 are on metamorphic zircons and 21 are on magmatic cores. $^{207}Pb/^{206}Pb$ ages of metamorphic zircons vary from 1813 to 1969 Ma with relatively low Th/U ratio of 0.007–0.1. These analyses yield a weighted mean $^{207}Pb/^{206}Pb$ age of 1898 ± 5 Ma (MSWD = 1.12) for metamorphism, which is consistent with an upper intercept age of 1917 ± 13 Ma (MSWD = 1.3) from a discordia trend (Fig. 7c). By contrast, magmatic cores have higher Th/U ratios from 0.46 to 0.83. Twenty-one spots show scattered $^{207}Pb/^{206}Pb$ ages from 1981 to 2128 Ma, yielding an upper intercept age of 2071 ± 20 Ma (MSWD = 1.7) (Fig. 7d). A weighted mean $^{207}Pb/^{206}Pb$ age of 2041 ± 7 Ma (MSWD = 1.5) is interpreted as the crystallization age of the protoliths, which is coeval with the age of magmatic cores in granitic gneiss samples jc20-0822–10 and jc20-0822–18.

Zircons from quartz schist sample jc21-1009–11 of the Longshoushan Complex are similar to zircons from the three granitic gneiss samples, but most grains show a core-rim structure with clear oscillatory features in cores (Fig. 6a). Unfortunately, the metamorphic rim is too thin to be analyzed. $^{207}Pb/^{206}Pb$ ages of 49 spots on zircon cores reveal a single age population from 1806 to 2205 Ma, resulting in the peak age at 2035 Ma (Fig. 8). The Th/U ratios of these spots are 0.13–1.16, indicating a magmatic origin. Only one concordant data spot gives $^{207}Pb/^{206}Pb$ age of 1806 ± 45 Ma with the high Th/U ratio of 0.89 (Table S2), different from the relatively low Th/U ratios in metamorphic zircons from the Longshoushan Complex (Gong et al., 2016; Zeng et al., 2018). Hence this data spot cannot constrain the timing of a later metamorphic event. The depositional age of this sample will be discussed later.

5.1.2. Age of the Dunzigou Group

Samples jc21-1009–10, jc21-1009–6, and jc21-1009–5 from the Dunzigou Group contain sub-rounded to rounded zircons with a length of ~ 50–200 μm and the length/width ratio of 1:1 to 3:1. Most zircon grains have oscillatory zoning and are relatively dark in CL images, and many grains are fractured (Fig. 6a). For quartzite sample jc21-1009–10, $^{207}Pb/^{206}Pb$ ages of 63 spots range from 1898 to 2674 Ma and show two age populations: 2.2–1.9 Ga with a peak age at 2044 Ma, and 2.45–2.2 Ga with a peak age at 2384 Ma (Fig. 9a and 9d). The Th/U rations of all spots are between 0.11 and 1.72.

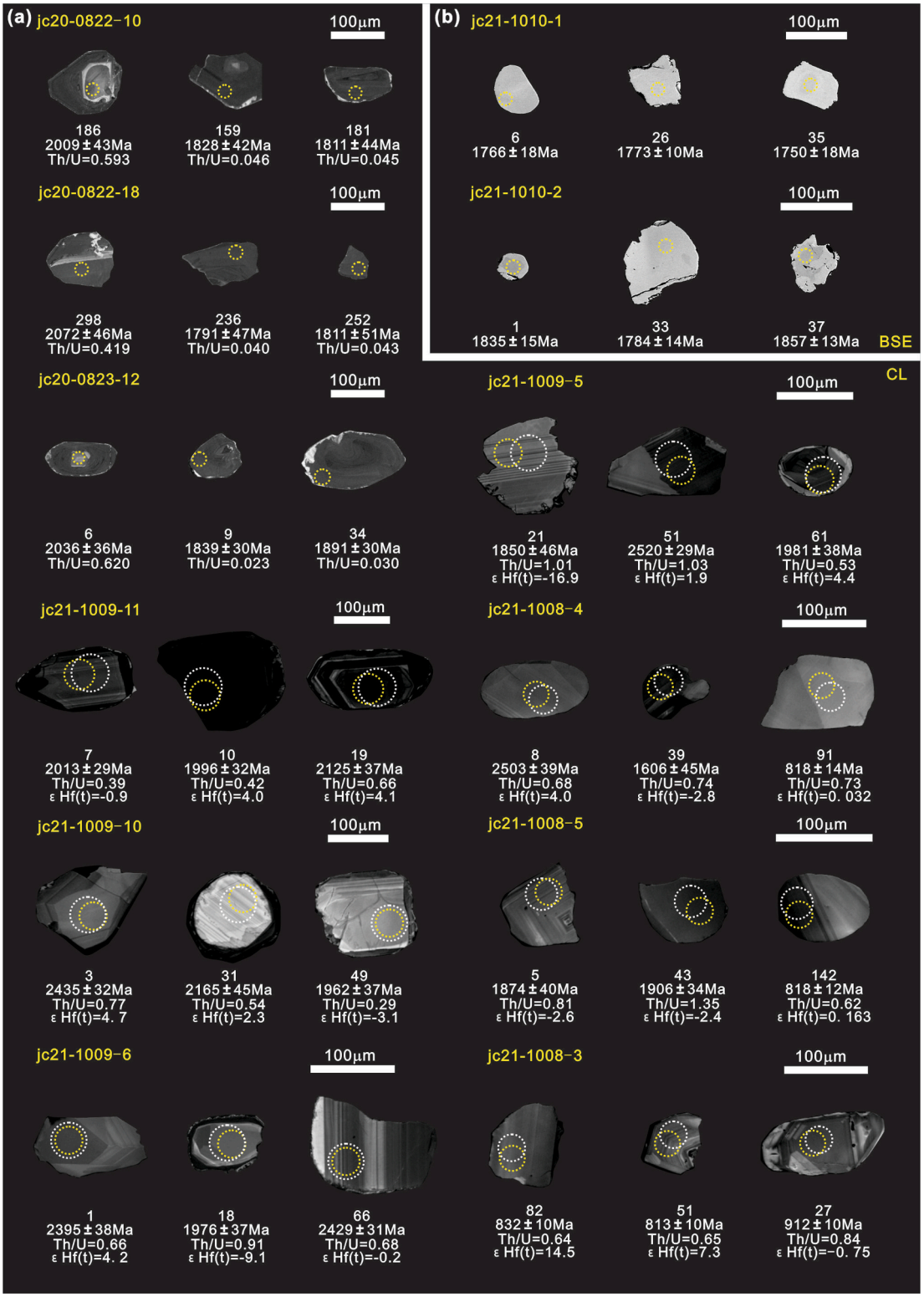

Fig. 6. Representative (a) CL images of dated zircon grains and (b) BSE images of monazite grains. Age with uncertainties at 1σlevel are indicated.

Zircons from quartz schist sample jc21-1009–6 were analyzed by 75 spots with Th/U ratio from 0.12 to 4.19. $^{207}Pb/^{206}Pb$ ages from 1676 to 2718 Ma show a bimodal population for these magmatic zircons: 2.0–1.8 Ga with a peak age at 1902 Ma and 2.65–2.3 Ga with a peak age at 2491 Ma (Fig. 9b and 9e).

Quartzite sample jc21-1009–5 were analyzed by 60 spots on 59 zircon grains. These spots have Th/U ratios from 0.29 to 2.07, and yield $^{207}Pb/^{206}Pb$ ages from 1770 to 2692 Ma. A bimodal population is characterized by 2.0–1.9 Ga with a peak age at 1896 Ma and 2.6–2.3 Ga with a peak age at 2457 Ma (Fig. 9e-f).

5.1.3. *Age of the Hanmushan Group*

Zircon grains from sandstone samples jc21-1008–4 and jc21-1008–5, and metasandstone sample jc21-1008–3 of the Hanmushan Group are

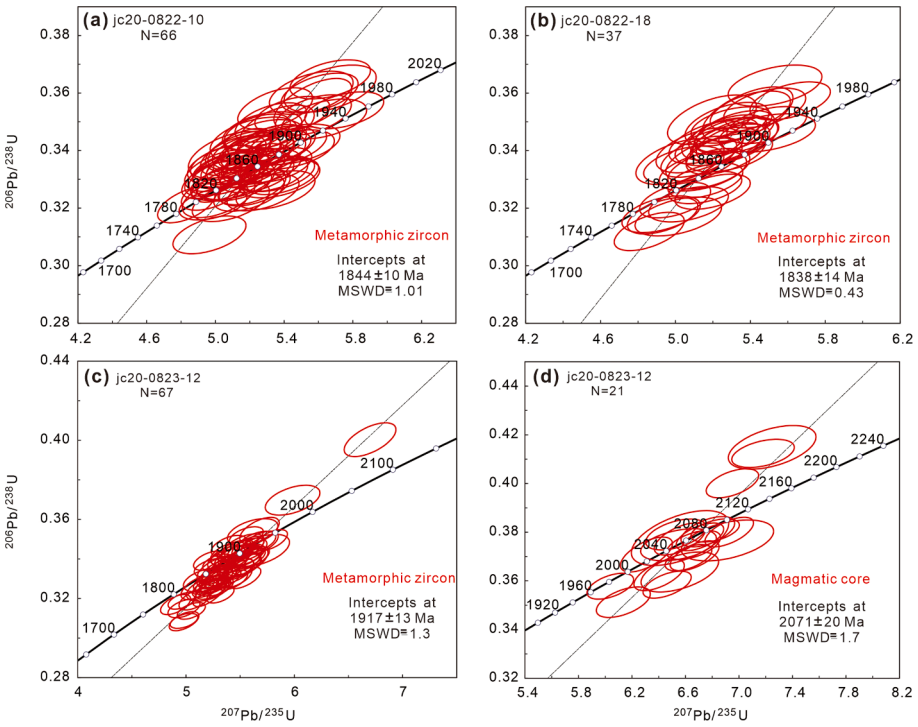

Fig. 7. U-Pb concordia diagrams for zircons from granitic gneiss samples of the Longshoushan Complex.

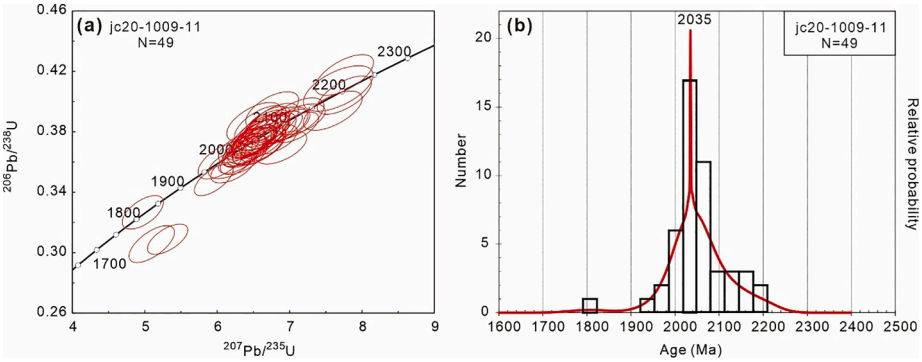

Fig. 8. (a) U-Pb concordia diagram and (b) Kernel Density Estimate (KDE) and histograms of detrital zircons from quartz schist sample of the Longshoushan Complex.

sub-prismatic to sub-rounded. Zircons from the two sandstone samples have the length of ~ 50–200 μm and the length/width ratio between 1:1 and 3:1, whereas zircons from sample jc21-1008–3 are smaller than 100 μm and the length/width ratio is between 1:1 and 2:1 (Fig. 6a). Detrital zircons from these samples under CL image show complex features. Some grains have clear oscillatory zoning whereas some are homogeneous.

Sample jc21-1008–4 were analyzed by 101 spots on 94 zircon grains, with the Th/U ratios between 0.16 and 2.36. Zircon ages range from 818 to 2687 Ma and can be divided into three age populations: the majority group of 2.6–2.3 Ga yields a peak age at 2484 Ma, the subordinate group of 2.2–1.5 Ga has a peak age at 1826 Ma, and the minor group of 0.9–0.7 Ga shows a peak age at 827 Ma (Fig. 10a and 10d). There is an age gap between 1500 and 900 Ma.

For sandstone sample jc21-1008–5, 153 spots on 138 zircon grains show the Th/U ratio from 0.15 to 2.16 and the ages from 818 to 2846 Ma. Similar to sample jc21-1008–4, detrital zircons from sample jc21-1008–5 also comprise three age populations: the majority group of 2.2–1.5 Ga with a peak age at 1869 Ma, the subordinate one of 2.8–2.2 Ga with a peak age at 2505 Ma, and the minor group from 0.9 to 0.8 Ga with a peak age at 846 Ma (Fig. 10b and 10e).

Metasandstone sample jc21-1008–3 were analyzed by 88 spots on 84 zircon grains, with the Th/U ratios between 0.18 and 2.73 and ages from 790 to 2939 Ma. Although the age distribution of detrital zircons from this sample can be divided into three age populations, the majority group is from 1.0 to 0.8 Ga with a peak age at 842 Ma. The subordinate group ranges from ca. 2.1 to 1.5 Ga with a peak age at 1838 Ma, and the minor group from ca. 2.7 to 2.3 Ga yields a peak age at 2475 Ma (Fig. 10c and 10f).

5.2. Zircon Lu-Hf isotopes

For quartz schist sample jc21-1009–11 from the Longshoushan Complex, 13 detrital zircons were analyzed for Hf isotope composition. Zircons with ages of 1.96 to 2.2 Ga have initial $^{176}Hf/^{177}Hf$ ratios from 0.281276 to 0.281614, corresponding to relatively positive εHf(t) values from −0.926 to 6.432 (Fig. 11a) with T^{C}_{DM} model ages of 2682–2290 Ma (Fig. 12a).

For the three metasedimentary samples from the Dunzigou Group, 63 detrital zircons were analyzed for the Hf isotope composition. Fifteen

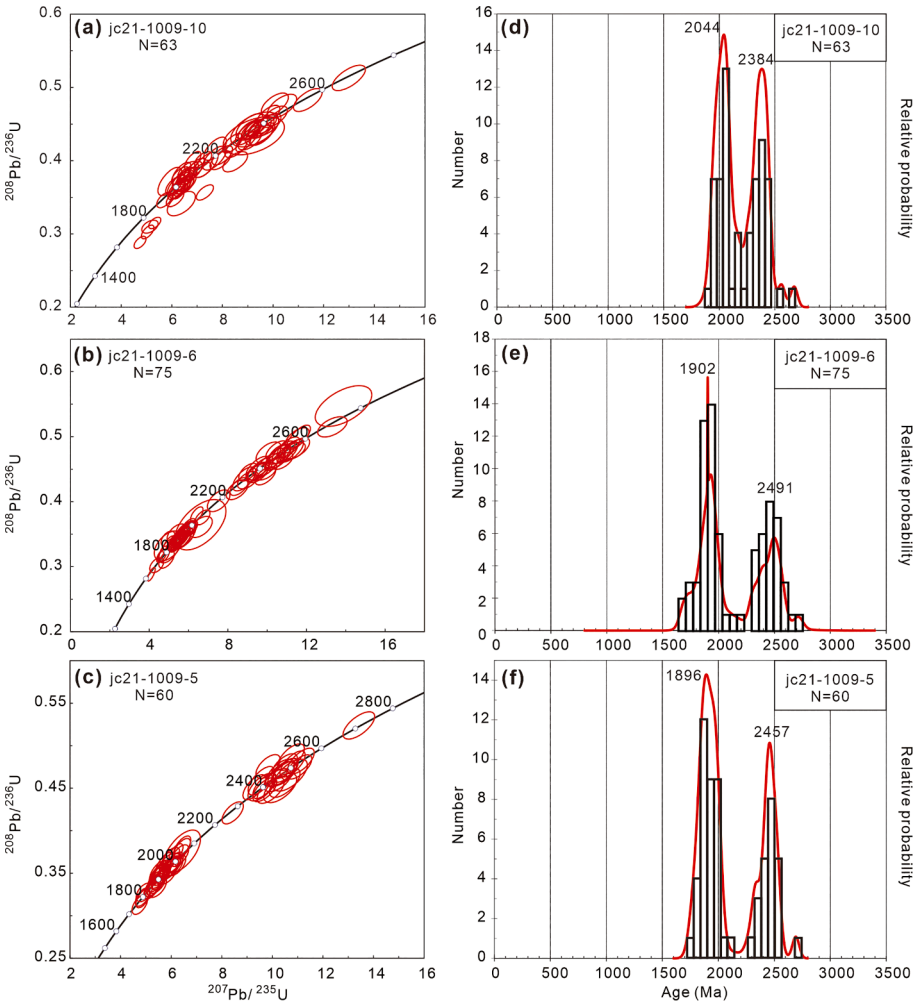

Fig. 9. U-Pb concordia diagrams (a-c), and Kernel Density Estimate and histograms (d-f) of detrital zircons from metasedimentary rock samples of the Dunzigou Group.

zircon grains from quartzite sample jc21-1009–10 show ages of 2.5–1.85 Ga and initial $^{176}Hf/^{177}Hf$ ratios from 0.281276 to 0.281614, corresponding to a relatively positive εHf(t) values from −3.09 to 8.105 (Fig. 11b) with T_{DM}^{C} model ages of 2445–2917 Ma (Fig. 12b). By contrast, 26 zircon grains from quartz schist sample jc21-1009–6 have ages of 2.7–1.7 Ga and initial $^{176}Hf/^{177}Hf$ ratios from 0.280879 to 0.281630, resulting in a broad array of εHf(t) values from −24.252 to 7.497 (Fig. 11b) with T_{DM}^{C} model ages of 4044–2446 Ma (Fig. 12b). Similar to sample jc21-1009–6, a broad array of εHf(t) values from −17.947 to 4.377 (Fig. 11b) is observed for 22 zircon grains from quartzite sample jc21-1009–5, which have ages of 2.6–1.7 Ga, initial $^{176}Hf/^{177}Hf$ ratios from 0.281047 to 0.281665, and T_{DM}^{C} model ages of 3677–2331 Ma (Fig. 12b).

For the samples from the Hanmushan Group, 148 detrital zircons were analyzed for the Hf isotope composition. For sandstone sample jc21-1008–4, 46 zircon grains with ages of 2.7–0.8 Ga have initial $^{176}Hf/^{177}Hf$ ratios from 0.281216 to 0.282335, corresponding to a wide range of εHf(t) values from −9.723 to 7.043 (Fig. 11c) with T_{DM}^{C} model ages of 3153–1565 Ma (Fig. 12c). 57 zircon grains from sandstone sample jc21-1008–5 with ages of 2.7–0.8 Ga have initial $^{176}Hf/^{177}Hf$ ratios from 0.280949 to 0.282262. They also form a wide range of εHf(t) values from −14.563 to 7.445 (Fig. 11c) with T_{DM}^{C} model ages of 3512–1724 Ma (Fig. 12c). Forty-five zircon grains from metasandstone sample jc21-1008–3 show ages of 2.9–0.7 Ga and initial $^{176}Hf/^{177}Hf$ ratios from 0.280977 to 0.282740, yielding a broad array of εHf(t) values from −15.177 to 16.138 (Fig. 11c) with T_{DM}^{C} model ages of 3518–701 Ma (Fig. 12c).

5.3. Monazite U-Th-Pb ages

Monazite grains from two mica schist samples of the Longshoushan Complex show a subhedral-anhedral shape and a homogenous texture (Fig. 6b), suggesting a metamorphic origin. Error ellipses are plotted at the 2σ confidence interval on a Tera-Wasserburg concordia diagram (Tera and Wasserburg, 1972), which has been colored corresponding to their Y concentration (Fig. 13). A total of 44 analyses on monazite from sample jc21-1010–1 show slightly higher Y concentration in older grains. This sample only preserves one thermal event with an intercept age of 1844 ± 16 Ma (MSWD = 3.8) (Fig. 13a). Similarly, 42 analyses on monazite from sample jc21-1010–2 reveal a thermal event with an intercept age of 1853 ± 17 Ma (MSWD = 5.7) (Fig. 13b).

6. Discussion

6.1. Ages of Proterozoic rocks in the Longshoushan area

6.1.1. Ages of crystallization and metamorphism for the Longshoushan Complex

The Longshoushan Complex in the Longshoushan area was traditionally divided into two sub-units: the lower part is the Baijiazuizi Unit intruded by the ~ 825 Ma Jinchuan mafic–ultramafic intrusion near Jinchang city, and the upper part is the Tamazigou Unit largely exposed

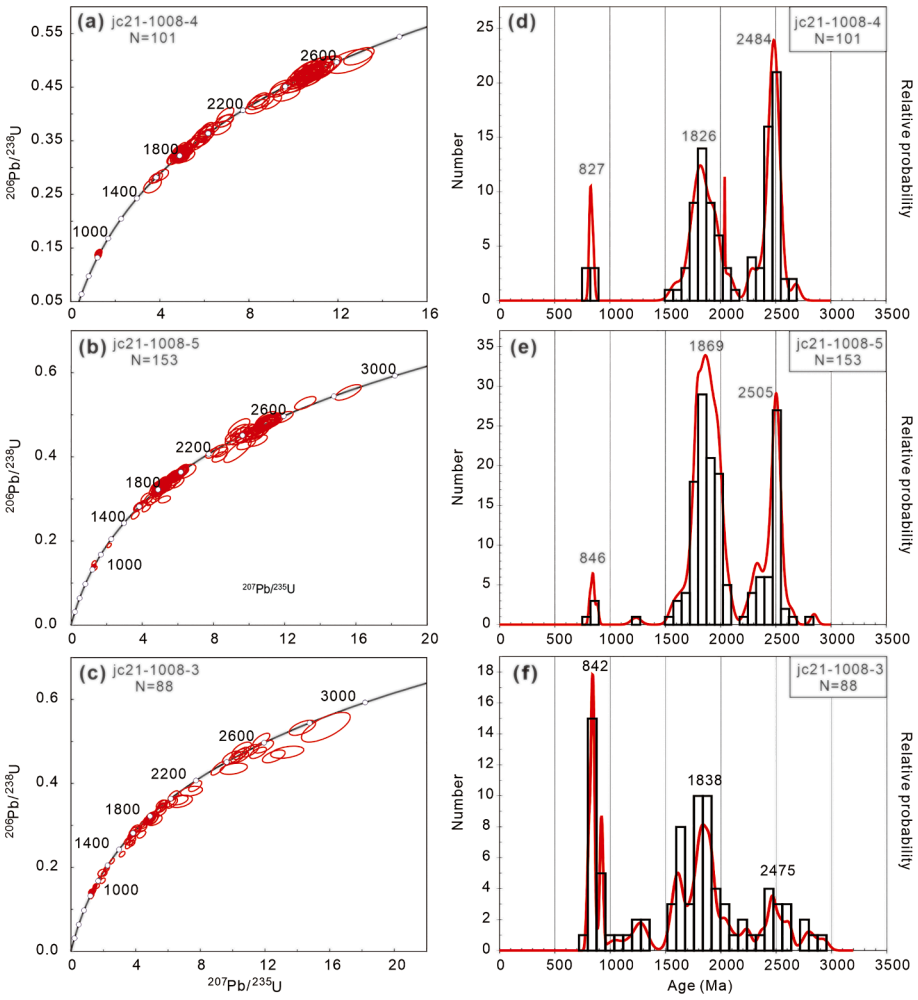

Fig. 10. (a-c) U-Pb concordia diagrams and (d-f) Kernel Density Estimate (KDE) and histograms of detrital zircons for the Hanmushan Group samples.

in the Dunzigou area, with an unconformity between the two units (Tung et al., 2007a; Yan et al., 2015a). The protolith ages of 2.3–1.9 Ga have been obtained for granite and granitic gneiss of the Longshoushan Complex near Jinchang city, yielding a peak at 2.1–2.0 Ga (Fig. 1b) (Xiu et al., 2002, 2004; Yan et al., 2015a; Gong et al., 2016; Zeng et al., 2018; Wu et al., 2021). In this study, the crystallization age of migmatite sample jc20-0823–12 is 2041 ± 7 Ma, coeval with the age of three magmatic zircon cores from granitic gneiss samples jc20-0822–10 and jc20-0822–18. This confirms that the protolith age of granitic gneiss of the Baijiazuizi Unit is ~ 2.0 Ga.

It is noteworthy that some analysis spots on zircons from the three granitic gneiss samples are above the concordant line in the concordia diagrams (Fig. 7a-c). This 'reverse discordance' phenomenon is defined by the $^{207}Pb/^{206}Pb$ age younger than U/Pb age evidently, which was also observed in samples near the Jinchuan intrusion (Gong et al., 2016; Zeng et al., 2018). Different from the discordance caused by Pb loss, the reverse discordance is due to genuine local excesses of 'unsupported' radiogenic Pb (Williams et al., 1984; Kusiak et al., 2013a,b). The change in the Pb mobility of the Longshoushan Complex may be caused by the disturbance of the U-Pb system during intrusion of the Jinchuan mafic–ultramafic rocks, as the re-distribution of radiogenic Pb in a ~ 4.3 Ga Jack Hills' zircon during a ~ 3.8 Ga or older event (Ge et al., 2018).

Here we summarize the metamorphic ages of the Longshoushan Complex from U-Pb ages of metamorphic zircons and monazite U-Th-Pb ages (Fig. 14). Taken into the analytical uncertainties of zircon ages, granitic gneiss, metagabbro and amphibolite from the Longshoushan Complex experienced two high-grade metamorphic events at ~ 1.95–1.90 Ga and ~ 1.85–1.80 Ga (Yan et al., 2015a; Gong et al., 2011, 2016; Zeng et al., 2018; This study). So far there are only one metamorphic zircon age of 1.95 Ga (Gong et al., 2016) and two monazite U-Th-Pb ages of ~ 1.85 Ga (Fig. 13) for metasedimentary rocks from the Longshoushan Complex. U-Th-Pb ages of monazite are often used to constrain the timing of a thermal event under upper amphibolite to granulite facies metamorphism (Parrish, 1990). Hence metasedimentary rocks and the underlying orthogneiss of the Longshoushan Complex experienced metamorphism together. The lack of ~ 1.8 Ga metamorphic age in metasedimentary rocks may be due to limited zircon growth. The unconformity between the Longshoushan Complex and the Dunzigou Group should be formed after the latest metamorphism at ~ 1.8 Ga. The metamorphic ages of 1.95–1.80 Ga are also found in the Diebusige and the Bayanwulashan complexes in the northeastern Alxa block (Dan et al., 2012a; Wu et al., 2014).

6.1.2. *Depositional ages of Proterozoic (meta)sedimentary rocks*

There are several methods to constrain the depositional ages of (meta)sedimentary rocks from detrital zircons. For example, detrital zircon U-Pb geochronology has been used to constrain the maximum depositional age of Precambrian rock units (Dickinson and Gehrels, 2009a). Coutts et al. (2019) tested 10 commonly-used calculation methods for the maximum depositional age and found that the Youngest Single Grain method and the Youngest Detrital Zircon method are more successful when applied to low uncertainty and datasets with small numbers of 50–120, which agree with the results by Dickinson and

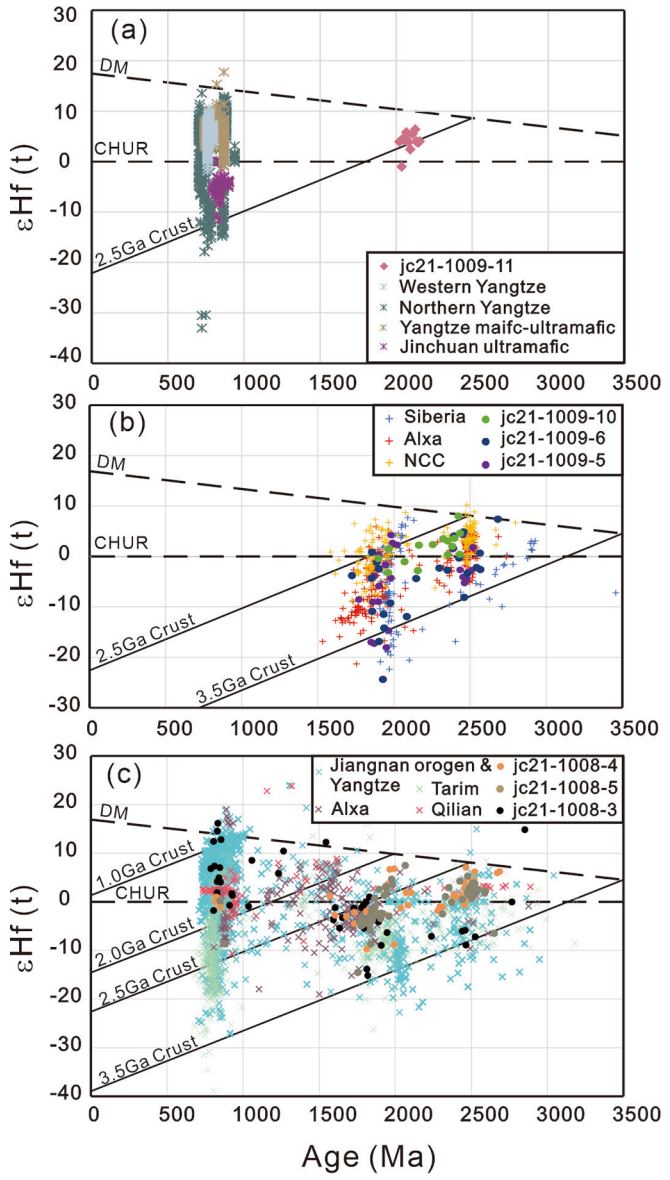

Fig. 11. U-Pb ages vs. εHf (t) values for detrital zircons of the Proterozoic samples from the Longshoushan area, compared with published data for other blocks. (a) Zircons from the Paleoproterozoic Longshoushan Complex sample jc21-1009–11 and Neoproterozoic magmatic rocks: Jinchuan ultramafic intrusion (Jiao et al., 2014; Tang et al., 2014; Duan et al., 2016; Xiao et al., 2019) and the Yangtze craton (Zhao et al., 2018b); (b) Detrital zircons from the Late Paleoproterozoic to the Early Mesoproterozoic sedimentary rocks: the Alxa block (Liu et al., 2019), Longshoushan (this study), NCC (Liu et al., 2017; Zhou et al., 2017), northern Siberia (Priyatkina et al., 2016); (c) Detrital zircons from the Neoproterozoic sedimentary rocks: Longshoushan (this study), the Alxa block (Liu et al., 2019; Tian et al., 2019), the Jiangnan orogenic belt (Wang et al., 2014), the Qilian orogenic belt (Yan et al., 2015b; Li et al., 2020; Gao et al., 2021), the Tarim craton (He et al., 2014a, b; Zhang et al., 2016a), and the Yangtze craton (Sun et al., 2009; Wang et al., 2012, Wang and Zhou, 2012; Wang et al., 2013; Zhang et al., 2015c). Abbreviations: DM: Depleted Mantle; CHUR: Chondrite.

Gehrels (2009b). However, Vermeesch (2021) recommended to use the 'Maximum Likelihood Age' (MLA) algorithm of Galbraith and Laslett (1993) and Galbraith (2005), which is built on solid statistical foundation and can converge to the correct solution with increasing sample size. Therefore, we adopt the MLA method to obtain the maximum depositional ages of our samples using the online software IsoplotR (Vermeesch, 2018).

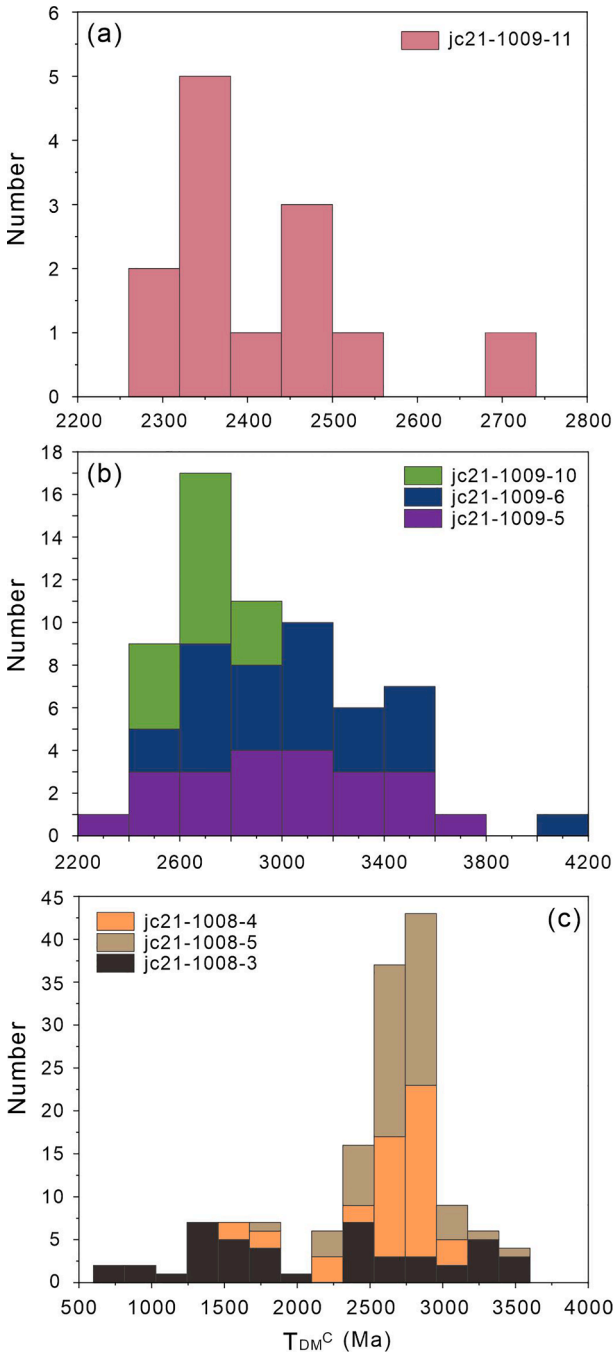

Fig. 12. The histogram of Hf isotope model age of samples from (a) the Longshoushan Complex, (b) the Dunzigou Group, and (c) the Hanmushan Group.

Depositional ages of Proterozoic (meta)sedimentary rocks in the Longshoushan area are poorly constrained so far. Quartz schist sample jc21-1009–11 from the Dunzigou area is located at the uppermost Longshoushan Complex (Fig. 3). Most detrital zircon grains of this sample show a core-rim structure. The detrital zircon ages yield a magmatic origin with the peak age at 2035 Ma (Fig. 8), suggesting the provenance from the underlying granitic gneiss in the Baijiazuizi Unit. The MLA of sample jc21-1009–11 is 1979.7 ± 50.5 Ma (Fig. 15a), which is older than the maximum depositional ages of 1868–1801 Ma for quartz schists from the Tamazigou Unit using the Youngest Three Zircons method (Gong et al., 2016; Liu et al., 2020a; Wu et al., 2021). As mentioned above, metasedimentary rocks of the Longshoushan Complex

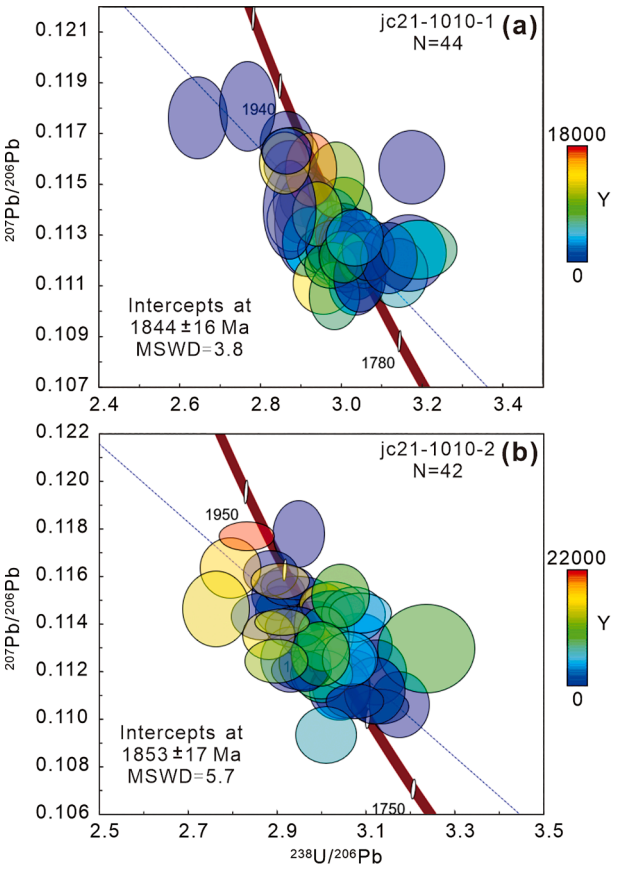

Fig. 13. Tera-Wasserburg concordia diagrams for U-Th-Pb data of monazite from mica schist samples of the Longshoushan Complex.

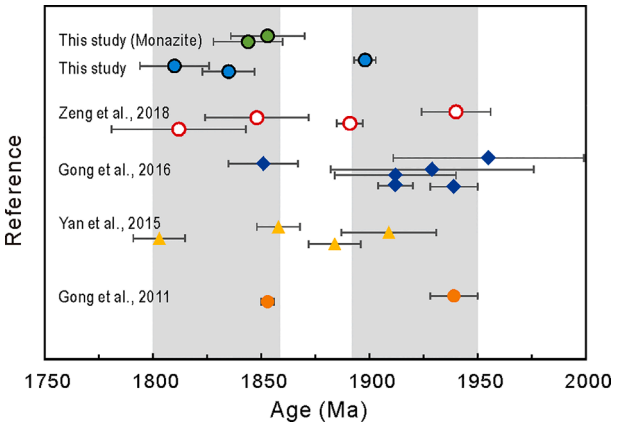

Fig. 14. Comparison of metamorphic ages of the Longshoushan Complex in the southwestern Alxa block. Except two monazite U-Th-Pb ages from this study, all data are from U-Pb ages of metamorphic zircons.

experienced metamorphism at ~ 1.95–1.90 Ga and ~ 1.85–1.80 Ga (Fig. 14), which allows us to constrain the depositional age of the protoliths between 1.98 and 1.95 Ga.

Li (1991) reported a Rb-Sr whole-rock isochron age of 1261 ± 22 Ma for the Dunzigou Group, hence the Dunzigou Group in the Longshoushan area is generally regarded as Mesoproterozoic sedimentary sequence (e.g., Gong et al., 2016; Wu et al., 2021, 2022). However, quartzite sample jc21-1009–10 from the basal conglomerate of the Dunzigou Group (Fig. 4f) yields the MLA of 2023.31 ± 18.94 Ma and without grains younger than 1.9 Ga (Fig. 15b). The MLA of quartz schist jc21-1009–6 and quartzite jc21-1009–5 are 1685.8 ± 135.8 Ma and 1881.7 ± 22.6 Ma, respectively (Fig. 15c-d), which are comparable with the maximum depositional age (1.75–1.67 Ga) of the Dunzigou Group from three youngest concordant zircon grains (Wu et al., 2021). Because the Dunzigou Group did not show high-grade metamorphism, deposition of the Dunzigou Group may occur in the Late Paleoproterozoic (1.8–1.7 Ga), just after formation of the unconformity between the Longshoushan Complex and the Dunzigou Group. It is worthy to note that the Dunzigou Group in the Longshoushan area were strongly folded, which may cause the older MLA for sample jc21-1009–5 than the apparently 'underlying' sample jc21-1009–6. The MLA of the Neoproterozoic Hanmushan Group samples jc21-1008–4, jc21-1008–5 and jc21-1008–3 is 831.83 ± 9.81 Ma, 845.44 ± 12.24 Ma and 829.5 ± 6.16 Ma, respectively (Fig. 15e-15 g).

6.2. *Provenance of Proterozoic rocks in the Longshoushan area*

6.2.1. *Provenance of the Longshoushan Complex and Dunzigou Group*

For the Longshoushan Complex, the single age distribution of detrital zircon ages from quartz schist sample jc21-1009–11 (Fig. 8b) is comparable with the detrital zircon age spectra with a peak at ~ 2.03 Ga from coeval sedimentary rocks in the Khondalite belt (Dan et al., 2012b, and references therein). Zircon Lu-Hf isotope compositions can further distinguish zircons with the same crystallization age but formed in crustal domains that had separated from the mantle at different periods (Scherer et al., 2007; Wu et al., 2007). Similar to metasedimentary samples of the Longshoushan Complex from Gong et al. (2016), most zircon grains in quartz schist sample jc21-1009–11 show positive εHf(t) values lower than the depleted mantle evolution line (Fig. 11a). Combined with the T_{DM}^{C} values of 2.7–2.3 Ga, the provenance of Paleoproterozoic metasedimentary rocks of the Longshoushan Complex was also comparable with khondalites (Dan et al., 2012b).

Although the three metasedimentary samples from the Dunzigou Group show a bimodal distribution of detrital zircon ages, it is interesting to notice that the age peaks and Hf isotope compositions of zircons are different (Fig. 9). Sample jc21-1009–10 from the conglomerate layer at the bottom of the Dunzigou Group shows the peak ages at ~ 2.4 Ga and ~ 2.0 Ga (Fig. 9d), with positive εHf(t) values for most zircon grains (Fig. 11b). Compared with zircon ages and Hf isotope of the Longshoushan Complex (Gong et al., 2016; Zeng et al., 2018; this study), the Beidashan Complex (Zhang et al., 2013b), the Diebusige Complex and the Bayanwulashan Complex (Dan et al., 2012a; Wu et al., 2014), zircons of sample jc21-1009–10 were mainly provided by the Alxa block itself.

By contrast, samples jc21-1009–6 and jc21-1009–5 from the Dunzigou Group show two dominant zircon age groups at ~ 2.5 Ga and ~ 1.9 Ga (Fig. 9e and 9f), which are well recorded in the coeval strata from different blocks (Fig. 16a). The Paleoproterozoic basement of the Alxa block also contains coeval granites in Beidashan (~2.5 Ga, Zhang et al., 2013b), Longshoushan (~2.3–1.9 Ga, Gong et al., 2016, this study), and Bayanwulashan areas (~2.3 Ga, Dan et al., 2012a). Meanwhile, the two age groups could correspond to the Wutai (2.5–2.4 Ga) and Lüliang (2.4–1.8 Ga) movements in the NCC (Ma and Wu, 1981; Zhao and Cawood, 2012). Most zircon grains from the two samples exhibit negative εHf(t) values, especially those younger than 2.0 Ga and older than 2.4 Ga. However, the ~ 1.85 Ga grains with very negative εHf(t) values below −10 from the Dunzigou Group have not been reported in the NCC (Liu et al., 2020a), but are similar to zircons from the northern Siberian craton (Fig. 11b). Therefore, we propose that besides the Alxa block, other blocks such as the NCC and the northern Siberian craton could also provide detritus to the lower Dunzigou Group.

The change of source area in the three samples from the Dunzigou Group may occur between 1.8 and 1.7 Ga, according to their depositional ages. The T_{DM}^{C} model age indicates that the source area is clustered at 3.0–2.4 Ga for sample jc21-1009–10 but is more dispersive for the other two samples (Fig. 12b). This implies that the proportion of the

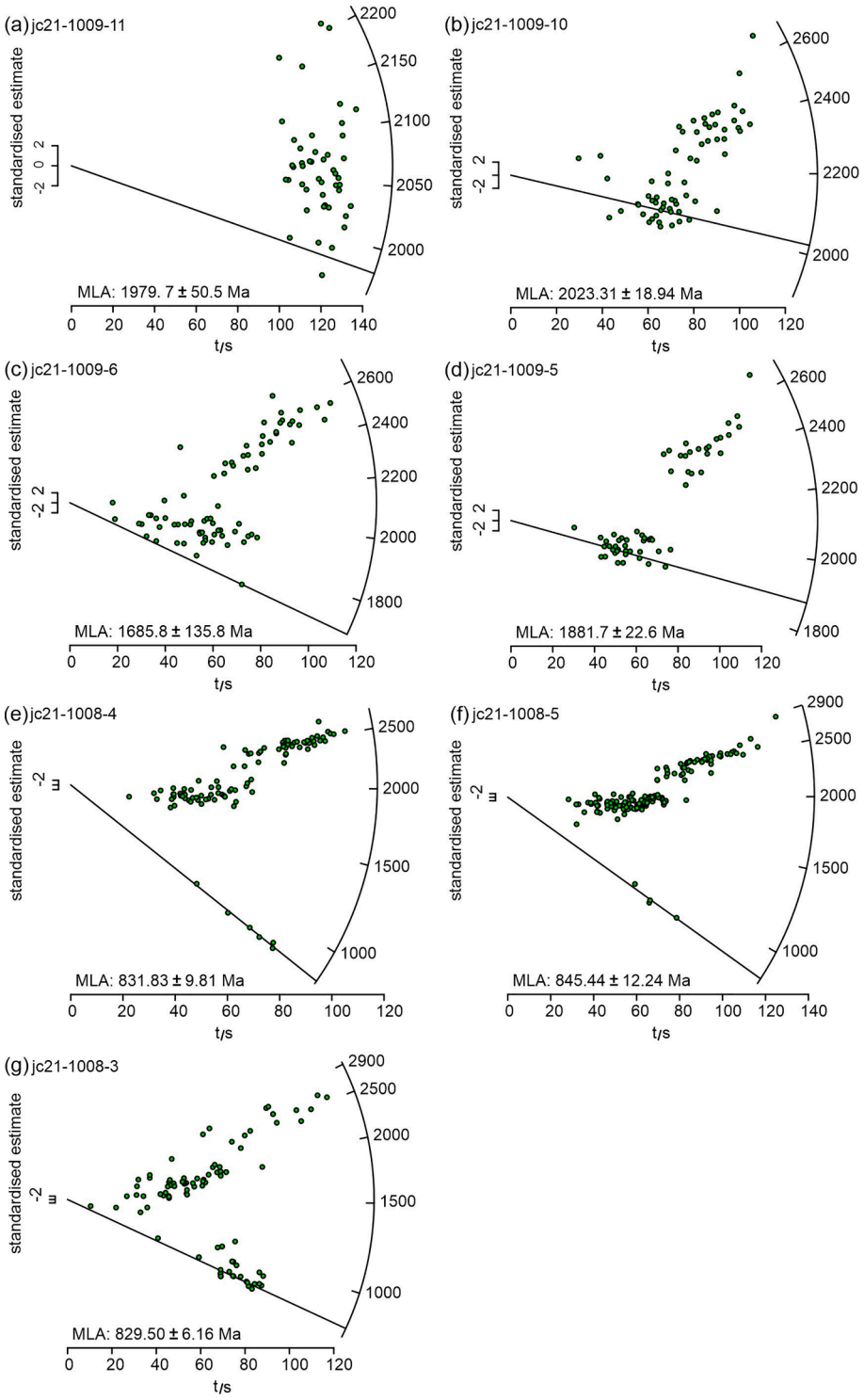

Fig. 15. The Maximum Likelihood Age (MLA) of Proterozoic samples from the Longshoushan area.

reworked Archean-Paleoproterozoic crust detritus increased in the Late Paleoproterozoic in the Longshoushan area.

6.2.2. *Provenance of the Hanmushan Group*

For the Hanmushan Group, detrital zircons from sandstone samples jc21-1008–4 and jc21-1008–5 are characterized by two dominant age peaks at 2.5 Ga and 1.9–1.8 Ga and a small peak at ~ 0.8 Ga. However, metasandstone sample jc21-1008–3 has the strongest Neoproterozoic age peak at 842 Ma, two minor peaks at 2.5 Ga and ~ 1.8 Ga, and continuous zircon ages from 1.5 to 0.9 Ga (Fig. 10d-f). The three samples show very close MLA from 830 to 845 Ma (Fig. 15e-g). The Neoproterozoic age peak at ~ 1.0–0.8 Ga has been attributed to the assembly and breakup of the Rodinia supercontinent (Li et al., 2008; Zhao et al., 2018a) and was preserved in detrital zircons from several cratons such as the South China block and the Tarim craton (Fig. 16b). The distinct age patterns of the Hanmushan Group and the Qingbaikou System in the NCC (Fig. 16b) demonstrate different source areas for the two units during the Early Neoproterozoic. Detrital zircon ages and Hf isotopes from the Langshan Group in the eastern Alxa block also indicate that the Alxa block was not a part of the NCC in the Neoproterozoic (Tian

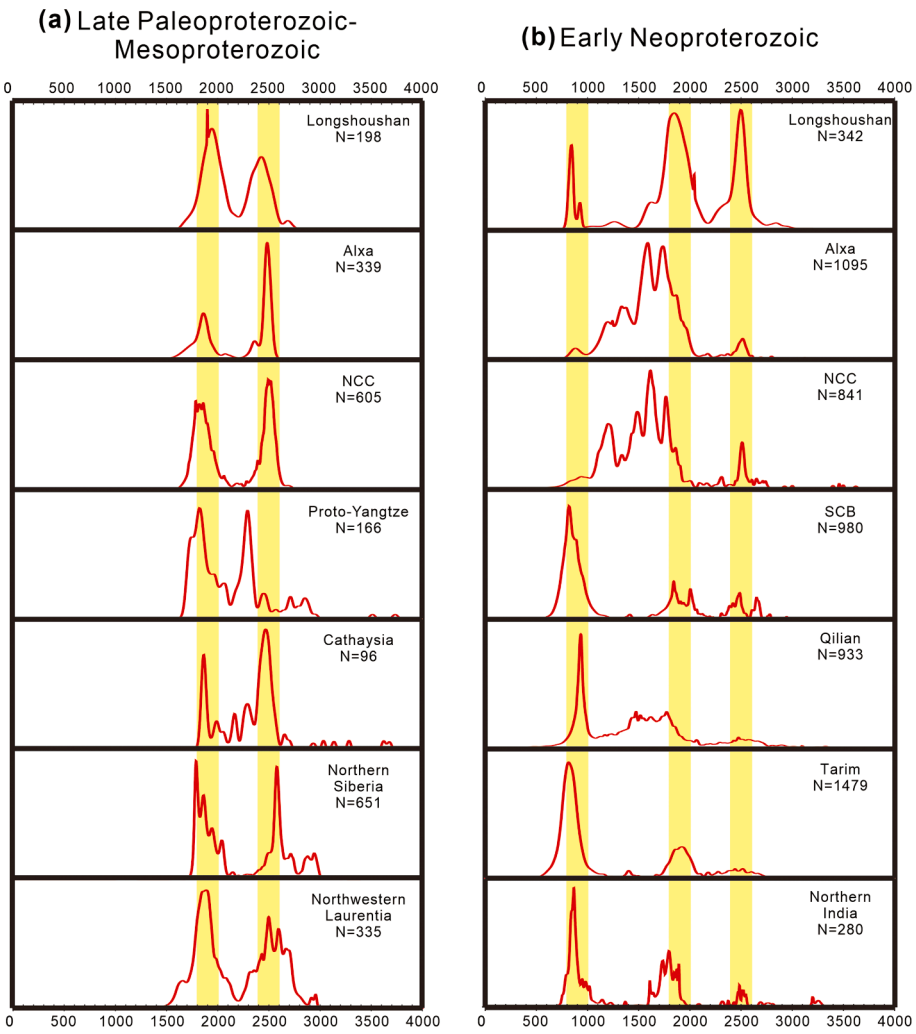

Fig. 16. (a) Age distributions of detrital zircons from Late Paleoproterozoic to Mesoproterozoic sedimentary rocks: Longshoushan (this study), the Alxa block (our results in the Longshoushan area are not included) (Liu et al., 2019); NCC (the North China Craton) (Liu et al., 2017, 2020; Yang et al., 2012b; Zhong et al., 2015; Zhou et al., 2017); Proto-Yangtze block (Zhao et al., 2010a); Cathaysia (Yu et al., 2012); Northern Siberia (Priyatkina et al., 2016); northwestern Laurentia (Furlanetto et al., 2016); (b) Age distributions of detrital zircons from Neoproterozoic sedimentary rocks: Longshoushan (this study), the Alxa block (our results in the Longshoushan area are not included) (Song et al., 2017; Liu et al., 2019; Tian et al., 2019); NCC (Sun et al., 2012; Hu et al., 2012; Yang et al.,2012a; Liu et al., 2020); South China block (SCB) (Liu et al., 2008; Sun et al., 2009; Wang et al., 2012, Wang and Zhou, 2012); Qilian (Gehrels et al., 2003; Tung et al., 2007b; Yan et al., 2015b; Li et al., 2019; Li et al., 2020; Gao et al., 2021); Tarim (He et al., 2014a, b; Zhang et al., 2016a); northern India (Spencer et al., 2012; Turner et al., 2014).

et al., 2019).

In addition, the Hf isotope composition of sandstone samples jc21-1008–4 and jc21-1008–5 is similar to the coeval strata in the Qilian orogenic belt, whereas *meta*-sandstone sample jc21-1008–3 contains a few grains at 1.6–1.0 Ga with positive εHf(t) and some grains at ~ 0.8 Ga with very positive εHf(t) values approaching the depleted mantle evolution line (Fig. 11c). The model age T_{DM}^{C} exhibits an age peak at 3.0–2.4 Ga for samples jc21-1008–4 and jc21-1008–5 but a wide distribution for sample jc21-1008–3 (Fig. 12c), suggesting the change of the source area of the Hanmushan Group in the Early Neoproterozoic. The Early Neoproterozoic juvenile crust materials for sample jc21-1008–3 have not been found in the Alxa block and cannot be provided by the Jinchuan intrusion with negative εHf(t) values (Jiao et al., 2014). However, the Yangtze craton has magmatic rocks at 0.9–0.8 Ga with the same Hf isotope composition (Fig. 11a). The ~ 0.8 Ga juvenile crust materials in sample jc21-1008–3 might derive from the Panxi-Hannan accretionary orogenic belt in the northwest Yangtze craton (Yao et al., 2019).

Interestingly, although the Paleoproterozoic (Xiu et al., 2002, 2004; Yan et al., 2015a; Gong et al., 2016; Zeng et al., 2018; Wu et al., 2021, this study), Mesoproterozoic (Song, 2014; Shi et al., 2016), and Neoproterozoic magmatic events (Dan et al., 2014; Hu et al., 2014; Xiao et al., 2015; Zhang et al., 2016c) are well preserved in the Alxa block, detrital zircon ages of the Neoproterozoic strata in the Alxa block show different patterns. Song et al. (2017) investigated the Hanmushan Group in the northwestern edge of the Longshoushan area and obtained the maximum depositional age at ~ 550 Ma with age peaks at ~ 0.8 Ga, ~1.0 Ga and ~ 2.5 Ga for two samples, and ~ 960 Ma with age peaks at ~ 1.2 Ga and ~ 1.4 Ga for one sample. They suggested that neither the Beidashan, Longshoushan, nor the western NCC provides sediments to the westmost Alxa because of a lack of the Paleoproterozoic and Archean detritus. Compared with our results, Neoproterozoic metasedimentary rock samples from Song et al. (2017) may not belong to the Hanmushan Group, or different drainage systems provided contrasting provenance for the Alxa block.

6.3. *Tectonic evolution of the Alxa block during Proterozoic*

6.3.1. *Tectonic setting of Proterozoic sedimentary rocks in Longshoushan*

Tectonic setting of (meta)sedimentary rocks can provide important constraints on the evolution of a sedimentary basin. Cawood et al. (2012) proposed a method to differentiate tectonic settings of sediments based on the specific distribution of detrital zircon ages. However, this method is limited by the poorly constrained depositional age of the sedimentary rocks (Coutts et al., 2019; Vermeesch, 2021). Barham et al. (2022) found that sedimentary rocks deposited in convergent/active settings show more unimodal detrital zircon age populations with a dominance of young ages, whereas those in divergent/passive margin settings have more polymodal and varied detrital zircon age populations. They proposed a method to discriminate the convergent and divergent tectonic settings on the basis of detrital zircon age population characteristics alone, without need for depositional age information. This method discriminates different tectonic settings via the 10th to 50th percentile of detrital zircon age populations and a modified Chi^2-

distribution value. Given the uncertainty on the depositional ages of Proterozoic (meta)sedimentary rocks in the Longshoushan area, we applied the method of Barham et al. (2022) to discriminate the tectonic settings of our samples.

As shown in Fig. 17, quartz schist sample from the Paleoproterozoic Longshoushan Complex was deposited in a convergent tectonic setting (larger Chi^2 value), but (meta)sedimentary samples from the overlying Dunzigou and Hanmushan groups were deposited in a divergent tectonic setting (smaller Chi^2 value). The depositional age of 1.98–1.95 Ga for quartz schist from the Longshoushan Complex is coeval with the 2.1–1.8 Ga orogenic event during the assembly of the Columbia supercontinent (Zhao et al., 2002). The depositional age (1.8–1.7 Ga) of the lower Dunzigou Group samples was coeval with the Late Paleoproterozoic extensional event in the NCC (Peng et al., 2008; Han et al., 2020), the Siberian craton (Gladkochub et al., 2022), and other blocks in the supercontinent Columbia (Cawood et al., 2020 and references therein). The provenance change between the Longshoushan Complex and the Dunzigou Group reflects the tectonic transition of the Alxa block from a convergent to a divergent setting during the Late Paleoproterozoic, which corresponds to the regional unconformity between them. The depositional age (840–830 Ma) of the Hanmushan Group samples is close to the intrusion of Jinchuan mafic–ultramafic rocks at ~ 825 Ma, which was probably related with the Neoproterozoic mantle plume in South China (Li et al., 2005). The Jinchuan intrusion was formed from intrusion of high-Mg basaltic magma in a continental rift zone (Chai and Naldrett, 1992). Hence the Longshoushan area experienced a transition from a convergent setting in the Late Paleoproterozoic (~1.98–1.95 Ga) to a divergent setting in the Late Paleoproterozoic (1.8–1.7 Ga) and then intracontinental rifting in the Early Neoproterozoic (~830 Ma).

6.3.2. *Tectonic affinity of the Alxa block during Proterozoic*

The tectonic affinity of the Alxa block during the Proterozoic is still controversial because of its small size and widespread Cenozoic sediments. Traditionally, the Alxa block is considered as a part of the Yinshan block (Zhao et al., 2005; Zhao, 2009) or the Khondalite belt (Dong et al., 2007; Geng et al., 2010; Zhang et al., 2013b; Gong et al., 2016; Zhang and Gong, 2018). However, some researchers argue that the Alxa block could be an independent Paleoproterozoic terrane (Dan et al., 2012a; Wu et al., 2014) and collided with the NCC in the Late Neoproterozoic (Dong et al., 2017), the Late Paleozoic (Huang et al., 2000; Yuan and Yang, 2015b; Zhang et al., 2011, 2013a, 2016b; Dan et al., 2016) or the Mesozoic (Yuan and Yang, 2015a). The affinity of the Alxa block with the South China block during the Neoproterozoic in the Rodinia supercontinent was also proposed (Li et al., 2005; Song et al., 2017).

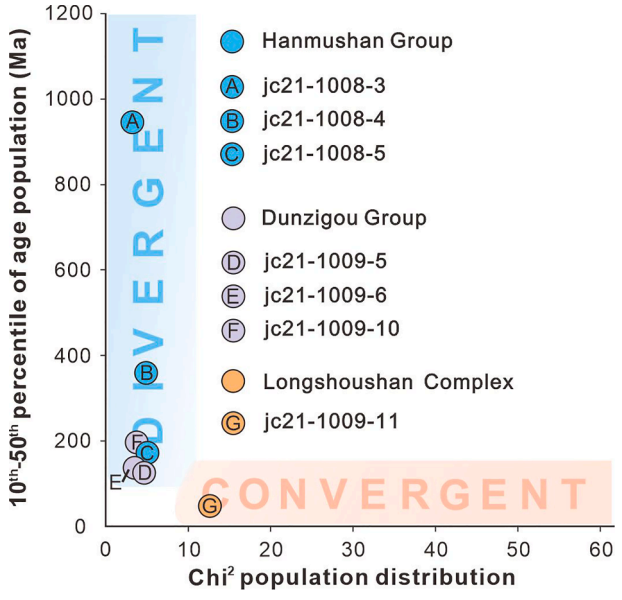

Fig. 17. Bivariate discrimination plot of active convergent and divergent/passive margin tectonic settings (Barham et al., 2022) for the Proterozoic samples in the Longshoushan area.

Based on paleomagnetic and geological records, the Paleo-Mesoproterozoic reconstruction models for the Columbia (Nuna) supercontinent have been proposed for major cratonic blocks (e.g., Zhao et al., 2002; Meert and Santosh, 2017; Cawood et al., 2020). The Paleoproterozoic rocks in the Alxa block underwent the magmatic events at ~ 2.5 Ga and ~ 2.3–2.0 Ga, and the metamorphic events at ~ 1.95–1.90 Ga and ~ 1.85–1.80 Ga (Zhang and Gong, 2018 and references therein; this study). The Late Paleoproterozoic metamorphic events have been recognized in nearly every continent, which was attributed to the assembly of the Columbia supercontinent (Zhao et al., 2002 and references therein). However, the Alxa block was not subjected to metamorphism at ~ 2.0 Ga, which is widely distributed in the center of the Columbia supercontinent including the proto-Yangtze block, northwest Laurentia, and southeast Siberian block (Cawood et al., 2018). Combined with the similar detrital zircon age spectra and Hf isotopes between the Alxa block and the Khondalite belt, the Alxa block may be located at the rim of the Columbia and connect with the Khondalite belt in the Late Paleoproterozoic (~1.98–1.95 Ga).

It is interesting to notice that the Huaian Complex at the conjunction of the Khondalite belt and Trans-North China Orogen records two metamorphic events: ~1.95 Ga metamorphism due to the collision zone between the Yinshan block and the Ordos block, and ~ 1.85 Ga metamorphism due to the collision between the Eastern and Western blocks (Zhao et al., 2010b). Although the former collision event fits well with the 1.95–1.90 Ga metamorphic event in the Longshoushan Complex, the latter cannot explain the widespread 1.85–1.80 metamorphic event in the Longshoushan Complex because the Alxa block is located in the westernmost of the NCC. Further investigations are needed to explain the tectonic meaning of 1.85–1.80 metamorphic event in the Alxa block.

In addition, the Dunzigou Group from the Alxa block have detrital zircon age patterns with two prominent peaks at ~ 2.5 Ga and ~ 1.9 Ga (Fig. 16a), which are also observed in the 1.8–1.6 Ga sedimentary rocks in the NCC, North Australia, northern Siberia, northern India, northwestern Laurentia and Cathaysia (Wuyi domain) (Fig. 16a; Cawood et al., 2020 and references therein). The Alxa block in the Late Paleoproterozoic was probably close to the NCC because the other blocks have additional age peaks. As discussed above, the zircon Hf isotope composition of the lower Dunzigou Group in the Longshoushan area is consistent with the NCC and Northern Siberia (Fig. 11b). Therefore, we suggest that the Alxa block was located between the NCC and northern Siberia at 1.8–1.7 Ga (Fig. 18a).

The Middle Mesoproterozoic rocks are mainly exposed in the Langshan area of the eastern Alxa block. Multiple Paleo-Mesoproterozoic age peaks at ~ 1.7 Ga, ~1.5 Ga and ~ 1.3 Ga in the Langshan Group (Zhang and Gong, 2018 and references therein) are comparable with coeval sedimentary rocks in the NCC (Liu et al., 2019), implying that the eastern Alxa block has a strong affinity with the NCC during the Middle Mesoproterozoic.

The deep time full-plate tectonic model of Merdith et al. (2021) reconstructed the tectonic evolution of micro-continental blocks (e.g., Alxa, Dunhuang, Central Qilian, and Qaidam) in East Asia from the Neoproterozoic to the Phanerozoic, which provides important constraints on the Neoproterozoic location of the Alxa block. The provenance of the Early Neoproterozoic Hanmushan Group in the Alxa block shows more similarity with the Yangtze craton as discussed above (Fig. 11c; Fig. 16b). In addition, the ~ 825 Ma Jinchuan ultramafic intrusion is generally thought to be the product of a mantle plume (Li et al., 2005), and belongs to the Guibei Large Igneous Province (LIP) event in the South China block (Ernst et al., 2008). A fragmented LIP formed at ~ 850–820 Ma in the northern margin of the Qaidam block may be also associated with the Neoproterozoic mantle plume in the

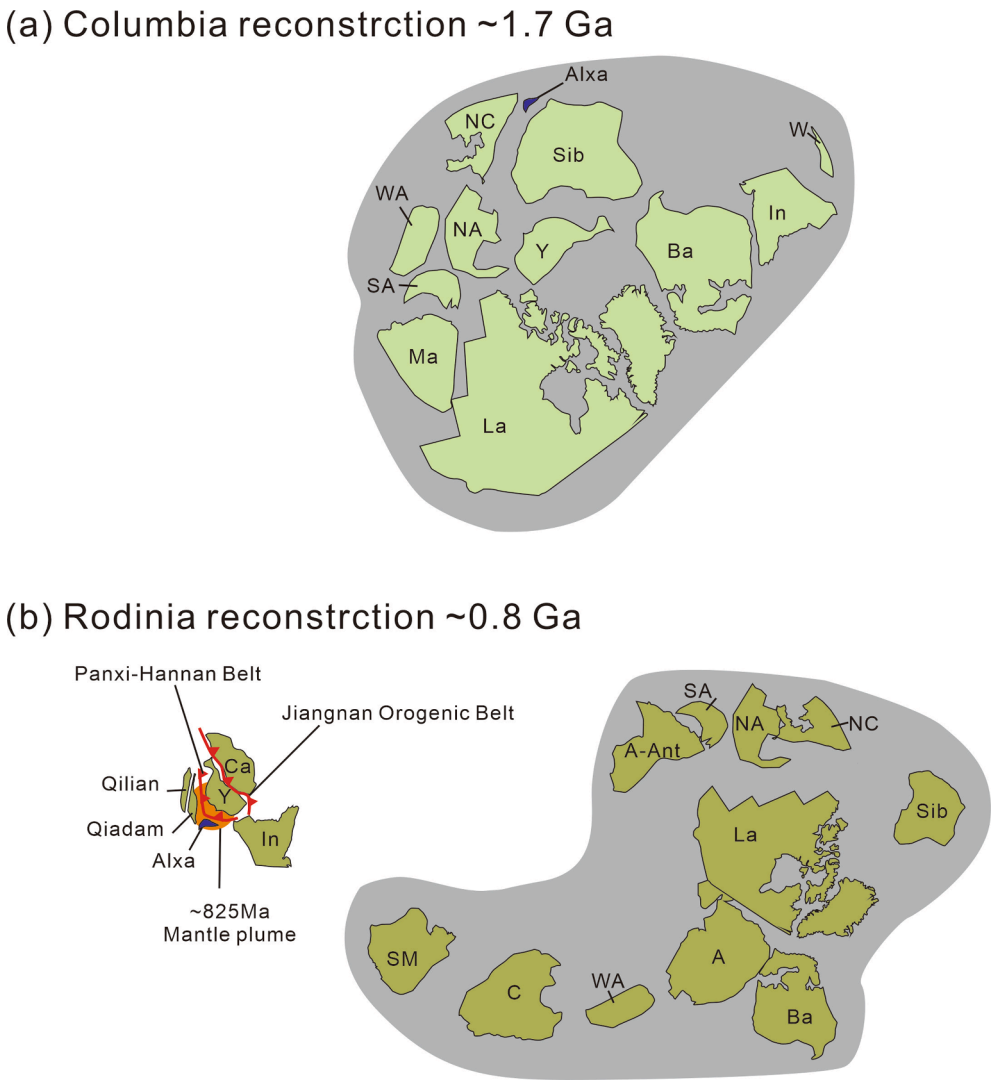

Fig. 18. Position of the Alxa block in (a) the Columbia supercontinent at ~ 1.7 Ga (modified after Cawood et al., 2020), and (b) the Rodinia supercontinent at ~ 0.8 Ga (modified after Merdith et al., 2021). Continent blocks: A, Amazonia; A-Ant, Austral-Antarctica; Ba, Baltic; C, Congo; Ca, Cathaysia; In, India; La, Laurentia; NA, North Australia; NC, North China; SA, South Australia; Sib, Siberia; SM, Sahara Metacraton; W, Wuyi domain; WA, West Australia; Y, Yangtze.

South China block (Xu et al., 2016). Therefore, we propose that the location of the Alxa block was close to the northwest Yangtze craton and the Qaidam block in the Early Neoproterozoic (Fig. 18b).

7. Conclusions

We systematically investigated U-Pb ages and Hf isotope composition of zircons and U-Th-Pb ages of monazite from Proterozoic rocks in the Longshoushan area in the southwestern Alxa block. The results indicate that the Paleoproterozoic Longshoushan Complex experienced a magmatic event at ~ 2.0 Ga and two metamorphic events at ~ 1.95–1.90 Ga and 1.85–1.80 Ga in a convergent setting, whereas the Late Paleoproterozoic Dunzigou Group and the Neoproterozoic Hanmushan Group deposited in a divergent setting at 1.8–1.7 Ga and intracontinental rifting at ~ 830 Ma, respectively. Combined with previous studies, the Alxa block experienced a long journey during the assembly and breakup of Columbia and Rodinia supercontinents. We propose that the Alxa block was connected with the Khondalite belt during the global orogenic event at 1.98–1.90 Ga. The Alxa block and the NCC may still stay together at 1.7 Ga. Their separation might take place in the Late Mesoproterozoic, because in the Early Neoproterozoic the NCC was located close to the eastern Laurentia whereas the Longshoushan area had a strong affinity with the northwestern Yangtze craton. Our results demonstrate that microcontinent blocks can provide the missing link to piecing together a jigsaw puzzle of supercontinents.

CRediT authorship contribution statement

Wenhao Su: Formal analysis, Investigation, Writing – original draft, Visualization. **Qin Wang:** Conceptualization, Investigation, Writing – review & editing, Supervision, Project administration, Funding acquisition. **Jian Kang:** Resources. **Xieyan Song:** Conceptualization, Resources, Funding acquisition.

Declaration of Competing Interest

The authors declare that they have no known competing financial interests or personal relationships that could have appeared to influence the work reported in this paper.

Data availability

The data in this research are presented in supplementary tables.

Acknowledgements

This work is supported by the Open Research Fund of the State Key Laboratory of Ore Deposit Geochemistry, Institute of Geochemistry, CAS (No. 202001) and the National Science Fund for Distinguished Young Scholars (No. 41825006). We thank help of Y. Wang and M. Long during field excursion. Constructive comments of two anonymous reviewers are helpful for revision of the manuscript.

Appendix A. Supplementary data

Supplementary data to this article can be found online at https://doi.org/10.1016/j.precamres.2023.107002.

References

Barham, M., Kirkland, C.L., Handoko, A.D., 2022. Understanding ancient tectonic settings through detrital zircon analysis. Earth Planet. Sci. 583, 117425 https://doi.org/10.1016/j.epsl.2022.117425.

BGGP (Bureau of Geology of Gansu Province), 1967. Regional Geology of the Gansu Province. Geological Publishing House Beijing (In Chinese).

Blichert-Toft, J., Albarède, F., 1997. The Lu–Hf geochemistry of chondrites and the evolution of the mantle-crust system. Earth Planet. Sci. 148, 243–258.

Cawood, P.A., Hawkesworth, C.J., Dhuime, B., 2012. Detrital zircon record and tectonic setting. Geology 40 (10), 875–878. https://doi.org/10.1130/G32945.1.

Cawood, P.A., Zhao, G.C., Yao, J.L., Wang, W., Xu, Y.J., Wang, Y.J., 2018. Reconstructing South China in Phanerozoic and Precambrian supercontinents. Earth Sci. Rev. 186, 173–194. https://doi.org/10.1016/j.earscirev.2017.06.001.

Cawood, P.A., Wang, W., Zhao, T.Y., Xu, Y.J., Mulder, J.A., Pisarevsky, S.A., Zhang, L.M., Gan, C.S., He, H.Y., Liu, H.C., Qi, L., Wang, Y.J., Yao, J.L., Zhao, G.C., Zhou, M.-F., Zi, J.-W., 2020. Deconstructing South China and consequences for reconstructing Nuna and Rodinia. Earth Sci. Rev. 204, 103169 https://doi.org/10.1016/j.earscirev.2020.103169.

Chai, G., Naldrett, A.J., 1992. The Jinchuan ultramafic intrusion: Cumulate of a high-Mg basaltic magma. J. Petrol. 33, 277–304.

Chu, N.-C., Taylor, R.N., Chavagnac, V., Nesbitt, R.W., Boella, R.M., Milton, J.A., German, C.R., Bayon, G., Burton, K., 2002. Hf isotope ratio analysis using multi-collector inductively coupled plasma mass spectrometry: an evaluation of isobaric interference corrections. J. Anal. At. Spectrom. 17, 1567–1574.

Coutts, D.S., Matthews, W.A., Hubbard, S.M., 2019. Assessment of widely used methods to derive depositional ages from detrital zircon populations. Geosci. Front. 10, 1421–1435.

Dan, W., Li, X.-H., Guo, J.H., Liu, Y., Wang, X.-C., 2012a. Paleoproterozoic evolution of the eastern Alxa Block, westernmost North China: evidence from in situ zircon U-Pb dating and Hf-O isotopes. Gondwana Res. 21, 838–864.

Dan, W., Li, X.-H., Guo, J.H., Liu, Y., Wang, X.-C., 2012b. Integrated in situ zircon U-Pb age and Hf-O isotopes for the Helanshan khondalites in North China Craton: juvenile crustal materials deposited in active or passive continental margin? Precambrian Res. 222–223, 143–158.

Dan, W., Li, X.-H., Wang, Q., Wang, X.-C., Liu, Y., 2014. Neoproterozoic S-type granites in the Alxa Block, westernmost North China and tectonic implications: In situ zircon U-Pb- Hf-O isotopic and geochemical constraints. Am. J. Sci. 314, 110–153.

Dan, W., Li, X.-H., Wang, Q., Wang, X.-C., Wyman, D.A., Liu, Y., 2016. Phanerozoic amalgamation of the Alxa Block and North China Craton: evidence from Paleozoic granitioids, U-Pb geochronology and Sr-Nd-Pb-Hf-O isotope geochemistry. Gondwana Res. 32, 105–121.

Dickinson, W.R., Gehrels, G.E., 2009a. Use of U-Pb ages of detrital zircons to infer maximum depositional ages of strata: a test against a Colorado Plateau Mesozoic database. Earth Planet. Sci. 288, 115–125.

Dickinson, W.R., Gehrels, G.E., 2009b. U-Pb ages of detrital zircons in Jurassic eolian and associated sandstones of the Colorado plateau: evidence for transcontinental dispersal and intraregional recycling of sediment. Geol. Soc. Am. Bull. 121, 408–433.

Dong, X.-P., Hu, J.-M., Li, Z.-H., Zhao, Y., Gong, W.-B., Yang, Y., 2017. Provenance of Ediacaran (Sinian) sediments in the Helanshan area, North China Craton: Constraints from U-Pb geochronology and Hf isotopes of detrital zircons. Precambrian Res. 298, 490–511. https://doi.org/10.1016/j.precamres.2017.06.022.

Dong, C.Y., Liu, D.Y., Li, J.J., Wan, Y.S., Zhou, H.Y., Li, C.D., Yang, Y.H., Xie, L.W., 2007. Paleoproterozoic Khondalite Belt in the western North China Craton: new evidence from SHRIMP dating and Hf isotope composition of zircons from metamorphic rocks in the Bayan Ul-Helan Mountains area. Chin. Sci. Bull. 52, 2984–2994.

Duan, J., Li, C.S., Qian, Z.Z., Jiao, J.G., Ripley, E.M., Feng, Y.Q., 2016. Multiple S isotopes, zircon Hf isotopes, whole-rock Sr-Nd isotopes, and spatial variations of PGE tenors in the Jinchuan Ni-Cu-PGE deposit, NW China. Miner Deposita 51, 557–574. https://doi.org/10.1007/s00126-015-0626-8.

Ernst, R.E., Wingate, M.T.D., Buchan, K.L., Li, Z.X., 2008. Global record of 1600–700Ma Large Igneous Provinces (LIPs): Implications for the reconstruction of the proposed Nuna (Columbia) and Rodinia supercontinents. Precambrian Res. 160, 159–178. https://doi.org/10.1016/j.precamres.2007.04.019.

Feng, J.Y., Xiao, W.J., Windley, B., Han, C.M., Wan, B.o., Zhang, J.E., Ao, S.J., Zhang, Z. Y., Lin, L.N., 2013. Field geology, geochronology and geochemistry of mafic–ultramafic rocks from Alxa, China: implications for Late Permian accretionary tectonics in the southern Altaids. J. Asian Earth Sci. 78, 114–142.

Furlanetto, F., Thorkelson, D.J., Rainbird, R.H., Davis, W.J., Gibson, H.D., Marshall, D. D., 2016. The Paleoproterozoic Wernecke SuperGroup of Yukon, Canada: Relationships to orogeny in northwestern Laurentia and basins in North America, East Australia, and China. Gondwana Res. 39, 14–40.

Galbraith, R.F., 2005. Statistics for Fission Track Analysis. CRC Press.

Galbraith, R.F., Laslett, G.M., 1993. Statistical models for mixed fission track ages. Nucl. Tracks Radiat. Meas. 21 (4), 459–470.

Gao, Y.L., Long, X.P., Luo, J., Dong, Y.P., Lan, C.Y., Huang, Z.Y., Zhao, J., 2021. Provenance and Hf isotopic variation of Precambrian detrital zircons from the Qilian Orogenic Belt, NW China: Evidence to the transition from breakup of Columbia to the assembly of Rodinia. Precambrian Res. 357, 106153 https://doi.org/10.1016/j.precamres.2021.106153.

Ge, R.F., Zhu, W.B., Wu, H.L., He, J.W., Zheng, B.H., 2013. Zircon U-Pb ages and Lu-Hf isotopes of Paleoproterozoic metasedimentary rocks in the Korla Complex, NW China: Implications for metamorphic zircon formation and geological evolution of the Tarim Craton. Precambrian Res. 231, 1–18.

Ge, R.F., Wilde, S.A., Nemchin, A.A., Whitehouse, M.J., Bellucci, J.J., Erickson, T.M., Frew, A., Thern, E.R., 2018. A 4463 Ma apparent zircon age from the Jack Hills (Western Australia) resulting from ancient Pb mobilization. Geology 46, 303–306. https://doi.org/10.1130/g39894.1.

Gehrels, G.E., Yin, A., Wang, X.-F., 2003. Detrital-zircon geochronology of the northeastern Tibetan plateau. Geol. Soc. Am. Bull. 115 (7), 881–896.

Geng, Y.S., Wang, X.S., Wu, C.M., Zhou, X.W., 2010. Late-Paleoproterozoic tectonothermal events of the metamorphic basement in Alxa area: evidence from geochronology. Acta Petrol. Sin. 26, 1159–1170 in Chinese with English abstract.

Gladkochub, D.P., Donskaya, T.V., Pisarevsky, S.A., Ernst, R.E., Söderlund, U., Kotov, A. B., Kovach, V.P., Okrugin, A.V., 2022. 1.79–1.75 Ga mafic magmatism of the Siberian craton and late Paleoproterozoic paleogeography. Precambrian Res. 370, 106557 https://doi.org/10.1016/j.precamres.2022.106557.

Gong, J.H., Zhang, J.X., Yu, S.Y., 2011. The origin of Longshoushan Group and associated rocks in the southern part of the Alxa Block: constraint from LA-ICP-MS U-Pb zircon dating. Acta Petrol. Mineral. 30, 795–818 in Chinese with English abstract.

Gong, J.H., Zhang, J.X., Yu, S.Y., Li, H.K., Hou, K.J., 2012. Ca. 2.5 Ga TTG rocks in the western Alxa Block and their implications. Chin. Sci. Bull. 57, 4064–4076.

Gong, J.H., Zhang, J.X., Wang, Z.Q., Yu, S.Y., Li, H.K., Li, Y.S., 2016. Origin of the Alxa Block, western China: New evidence from zircon U-Pb geochronology and Hf isotopes of the Longshoushan Complex. Gondwana Res. 36, 359–375.

Griffin, W.L., Wang, X., Jackson, S.E., Pearson, N.J., O'Reilly, S.Y., Xu, X.S., Zhou, X.M., 2002. Zircon chemistry and magma mixing, SE China: in situ analysis of Hf isotopes, Tonglu and Pingtan igneous complexes. Lithos 61 (3–4), 237–269.

Han, S.X., Wu, C., Zhou, Z.G., Wang, G.S., 2020. Geology, geochemistry, and geochronology of the paleoproterozoic Donggouzi mafic-ultramafic complex: Implications for the evolution of the North China craton. Lithos 366–367.

He, J.W., Zhu, W.B., Ge, R.F., Zheng, B.H., Wu, H.L., 2014a. Detrital zircon U-Pb ages and Hf isotopes of Neoproterozoic strata in the Aksu area, northwestern Tarim Craton: Implications for supercontinent reconstruction and crustal evolution. Precambrian Res. 254, 194–209. https://doi.org/10.1016/j.precamres.2014.08.016.

He, J.W., Zhu, W.B., Ge, R.F., 2014b. New age constraints on Neoproterozoic diamicites in Kuruktag, NW China and Precambrian crustal evolution of the Tarim Craton. Precambrian Res. 241, 44–60. https://doi.org/10.1016/j.precamres.2013.11.005.

Hu, J.M., Gong, W.B., Wu, S.J., Liu, Y., Liu, S.C., 2014. LA-ICP-MS zircon U-Pb dating of the Langshan Group in the northeast margin of the Alxa block, with tectonic implications. Precambrian Res. 225, 756–770.

Hu, H., Wang, R.C., Shao, C.J., Xie, L., Tian, E.N., Che, X.D., Yang, Z.Y., 2020. In situ LA-ICP-MS U-Th-Pb isotopic dating of monazite based on the monazite standard Trebilcock. J. Nanjing Univ. Natrual Sci. 56 (6), 763–773.

Hu, B., Zhai, M.G., Li, T.S., Li, Z., Peng, P., Guo, J.H., Kusky, T.M., 2012. Mesoproterozoic magmatic events in the eastern North China Craton and their tectonic implications: Geochronological evidence from detrital zircons in the Shandong Peninsula and North Korea. Gondwana Res. 22, 828–842. https://doi.org/10.1016/j.gr.2012.03.005.

Huang, B.C., Otofuji, Y.-I., Yang, Z.Y., Zhu, R.X., 2000. Preliminary result and itstectonic implications of middle Cambrian paleomagnetism in the Alxa and Hexi corridor terrane. Chin. J. Geophys. 43, 393–401 in Chinese with English abstract.

Jiao, J.G., Liu, H., Duan, J., Lu, H., Luo, D.Z., Qi, D., 2014. Hf Isotope Geochemical Characteristics and Magma Sources in Jinchuan Cu-Ni Sulfide Deposit. J. Earth Sci. Environ. 36, 58–67 in Chinese with English abstract.

Kusiak, M.A., Whitehouse, M.J., Wilde, S.A., Nemchin, A.A., Clark, C., 2013a. Mobilization of radiogenic Pb in zircon revealed by ion imaging: Implications for early Earth geochronology. Geology 41, 291–294. https://doi.org/10.1130/g33920.1.

Kusiak, M.A., Whitehouse, M.J., Wilde, S.A., Dunkley, D.J., Menneken, M., Nemchin, A. A., Clark, C., 2013b. Changes in zircon chemistry during Archean UHT metamorphism in the Napier Complex. Antarctica. Am. J. Sci. 313, 933–967. https://doi.org/10.2475/09.2013.05.

Kusky, T.M., 2011. Geophysical and geological tests of tectonic models of the North China Craton. Gondwana Res. 20, 26–35.

Kusky, T.M., Li, J.H., 2003. Paleoproterozoic tectonic evolution of the North China Craton. J. Asian Earth Sci. 22, 383–397.

Li, W.Y., 1991. The Sinian System in Longshoushan area. Northwest. Geol. 12 (2), 1–5 in Chinese.

Li, Z.X., Bogdanova, S.V., Collins, A.S., Davidson, A., De Waele, B., Ernst, R.E., Fitzsimons, I.C.W., Fuck, R.A., Gladkochub, D.P., Jacobs, J., Karlstrom, K.E., Lu, S., Natapov, L.M., Pease, V., Pisarevsky, S.A., Thrane, K., Vernikovsky, V., 2008.

Assembly, configuration, and break-up history of Rodinia: A synthesis. Precambrian Res. 160, 179–210. https://doi.org/10.1016/j.precamres.2007.04.021.
Li, J.H., Kroner, A., Qian, X.L., Brien, P.O., 2000. Tectonic Evolution of an Early Precambrian High-Pressure Granulite Belt in the North China Craton. Acta Geol. Sin. 74, 246–258.
Li, X.-H., Li, W.-X., Li, Z.-X., Lo, C.-H., Wang, J., Ye, M.-F., Yang, Y.-H., 2009. Amalgamation between the Yangtze and Cathaysia Blocks in South China: Constraints from SHRIMP U-Pb zircon ages, geochemistry and Nd–Hf isotopes of the Shuangxiwu volcanic rocks. Precambrian Res. 174, 117–128. https://doi.org/10.1016/j.precamres.2009.07.004.
Li, Z.Y., Li, Y.L., Xiao, W.J., Zheng, J.P., Brouwer, F.M., 2020. Geochemical and zircon U-Pb-Hf isotopic study of metasedimentary rocks from the Huangyuan Group of the Central Qilian block (NW China): Implications for paleogeographic reconstruction of Rodinia. Precambrian Res. 351, 105947.
Li, X.H., Su, L., Chung, S.-L., Li, Z.X., Liu, Y., Song, B., Liu, D.Y., 2005. Formation of the Jinchuan ultramafic intrusion and the world's third largestNi-Cu sulfide deposit: associated with the ~825 Ma South China mantle plume? Geochem. Geophys. Geosyst. 6, 1–16.
Li, S.Z., Suo, Y.H., Li, X.Y., Liu, B., Dai, L.M., Wang, G.Z., Wang, G., Zhou, J., Li, Y., Liu, Y.M., Cao, X.Z., Somerville, I., Mu, D.L., Zhao, S.J., Liu, J.P., Zhen, L.B., Zhao, L. T., Zhu, J.J., Yu, S.Y., Liu, Y.J., Zhang, G.W., 2018b. Microplate Tectonics: new insights from micro-blocks in the global oceans, continental margins and deep mantle. Earth Sci. Rev. 185, 1029–1064. https://doi.org/10.1016/j.jseaes.2011.06.
Li, X.H., Tang, G.Q., Gong, B., Yang, Y.H., Hou, K.J., Hu, Z.C., Li, Q.L., Liu, Y., Li, W.X., 2013. Qinghu zircon: A working reference for microbeam analysis of U-Pb age and Hf and O isotopes. Chin. Sci. Bull. 58, 4647–4654. https://doi.org/10.1007/s11434-013-5932-x.
Li, K.Z., Wang, J., Cui, X.Z., Hou, M.C., Deng, Q., Huang, Z.F., Wang, C., 2019. Early Neoproterozoic syncollisional S-type granites from the western Yangtze Block, South China: Implications for final closure of the back-arc basin. Episodes 42 (2), 119–133.
Li, S.Z., Zhao, S.J., Liu, X., Cao, H.H., Yu, S., Li, X.Y., Somerville, I., Yu, S.Y., Suo, Y.H., 2018a. Closure of the Proto-Tethys Ocean and Early Paleozoic amalgamation of microcontinental blocks in East Asia. Earth Sci. Rev. 186, 37–75. https://doi.org/10.1016/j.earscirev.2017.01.011.
Liu, X.M., Gao, S., Diwu, C.R., Ling, W.L., 2008. Precambrian crustal growth of Yangtze Craton as revealed by detrital zircon studies. Am. J. Sci. 308, 421–468. https://doi.org/10.2475/04.2008.02.
Liu, Y.S., Hu, Z.C., Zong, K.Q., Gao, C.G., Gao, S., Xu, J., Chen, H.H., 2010. Reappraisement and refinement of zircon U-Pb isotope and trace element analyses by LA-ICP-MS. Chin. Sci. Bull. 55, 1535–1546. https://doi.org/10.1007/s11434-010-3052-4.
Liu, J.N., Yin, C.Q., Zhang, J., Qian, J.H., Li, S., Xu, K.Y., Wu, S.J., Xia, Y.F., 2020b. Tectonic evolution of the Alxa Block and its affinity: Evidence from the U-Pb geochronology and Lu-Hf isotopes of detrital zircons from the Longshoushan Belt. Precambrian Res. 344, 105733 https://doi.org/10.1016/j.precamres.2020.105733.
Liu, C.H., Zhao, G.C., Liu, F.L., Shi, J.R., 2017. Detrital zircon U-Pb and Hf isotopic and whole-rock geochemical study of the Bayan Obo Group, northern margin of the North China Craton: Implications for Rodinia reconstruction. Precambrian Res. 303, 372–391. https://doi.org/10.1016/j.precamres.2017.04.033.
Liu, C.H., Zhao, G.C., Liu, F.L., Shi, J.R., 2019. Late Precambrian tectonic affinity of the Alxa block and the North China Craton: Evidence from zircon U-Pb dating and Lu-Hf isotopes of the Langshan Group. Precambrian Res. 332, 312–332. https://doi.org/10.1016/j.precamres.2017.10.019.
Liu, C.H., Zhao, G.C., Liu, F.L., Shi, J.R., Ji, L., 2020a. Detrital zircon records of late Paleoproterozoic to early Neoproterozoic northern North China Craton drainage reorganization: Implications for supercontinent cycles. Geol. Soc. Am. Bull. 132, 2135–2153. https://doi.org/10.1130/b35506.1.
Ludwig, K.R., 2012. Isoplot v. 3.75dA Geochronological Toolkit for Microsoft Excel, vol. 5. Berkeley Geochronology Center, Special Publication, pp. 1-75.
Ma, X.Y., Wu, Z.W., 1981. Early tectonic evolution of China. Precambrian Res. 14, 185–202.
Meert, J.G., Santosh, M., 2017. The Columbia supercontinent revisited. Gondwana Res. 50, 67–83. https://doi.org/10.1016/j.gr.2017.04.011.
Merdith, A.S., Williams, S.E., Collins, A.S., Tetley, M.G., Mulder, J.A., Blades, M.L., Young, A., Armistead, S.E., Cannon, J., Zahirovic, S., Müller, R.D., 2021. Extending full-plate tectonic models into deep time: Linking the Neoproterozoic and the Phanerozoic. Earth Sci. Rev. 214, 103477 https://doi.org/10.1016/j.earscirev.2020.103477.
Parrish, R.R., 1990. U-Pb dating of monazite and its application to geological problems. Can. J. Earth Sci. 27, 1431–1450.
Peng, P., Zhai, M.G., Ernst, R.E., Guo, J.H., Liu, F., Hu, B., 2008. A 1.78 Ga large igneous province in the North China craton: the Xiong'er volcanic province and the North China dyke swarm. Lithos 101, 260–280.
Porter, T.M., 2016. Regional tectonics, geology, magma chamber processes and mineralisation of the Jinchuan nickel-copper-PGE deposit, Gansu Province, China: A review. Geosci. Front. 7, 431–451. https://doi.org/10.1016/j.gsf.2015.10.005.
Priyatkina, N., Khudoley, A.K., Collins, W.J., Kuznetsov, N.B., Huang, H.-Q., 2016. Detrital zircon record of Meso- and Neoproterozoic sedimentary basins in northern part of the Siberian Craton: Characterizing buried crust of the basement. Precambrian Res. 285, 21–38. https://doi.org/10.1016/j.precamres.2016.09.003.
Scherer, E., Munker, C., Mezger, K., 2001. Calibration of the lutetium–hafnium clock. Science 293, 683–687.
Scherer, E.E., Whitehouse, M.J., Munker, C., 2007. Zircon as a Monitor of Crustal Growth. Elements 3, 19–24. https://doi.org/10.2113/gselements.3.1.19.
Shi, X.J., Zhang, L., Wang, T., Zhang, J.J., Liu, M.H., Zhou, H.S., Yan, Y.T., 2016. Zircon geochronology and Hf isotopic compositions for the Mesoproterozoic gneisses in Zongnaishan area, northern Alxa and its tectonic affinity. Acta Petrol. Sin. 32 (11), 3518–3536 in Chinese with English abstract.
Sláma, J., Košler, J., Condon, D.J., Crowley, J.L., Gerdes, A., Hanchar, J.M., Horstwood, M.S.A., Morris, G.A., Nasdala, L., Norberg, N., Schaltegger, U., Schoene, B., Tubrett, M.N., Whitehouse, M.J., 2008. Plešovice zircon—A new natural reference material for U-Pb and Hf isotopic microanalysis. Chem. Geol. 249 (1–2), 1–35. https://doi.org/10.1016/j.chemgeo.2007.11.005.
Song, W., 2014. Research on Precambrian metamorphosed plutonic intrusions in the Northern Alxa, Inner Mongolia. Master Degree Thesis. China University of Geosciences, Beijing, pp. 1–50 in Chinese with English summary.
Song, X.-Y., Danyushevsky, L.V., Keays, R.R., Chen, L.-M., Wang, Y.-S., Tian, Y.-L., Xiao, J.-F., 2012. Structural, lithological, and geochemical constraints on the dynamic magma plumbing system of the Jinchuan Ni–Cu sulfide deposit, NW China. Miner Deposita 47, 277–297. https://doi.org/10.1007/s00126-011-0370-7.
Song, D.F., Xiao, W.J., Collins, A.S., Glorie, S., Han, C.M., Li, Y.C., 2017. New chronological constrains on the tectonic affinity of the Alxa Block, NW China. Precambrian Res. 299, 230–243.
Spencer, C.J., Harris, R.A., Dorais, M.J., 2012. Depositional provenance of the Himalayan metamorphic core of Garhwal region, India: Constrained by U-Pb and Hf isotopes in zircons. Gondwana Res. 22, 26–35. https://doi.org/10.1016/j.gr.2011.10.004.
Sun, J.-F., Yang, J.-H., Wu, F.-Y., Wilde, S.A., 2012. Precambrian crustal evolution of the eastern North China Craton as revealed by U-Pb ages and Hf isotopes of detrital zircons from the Proterozoic Jing'eryu Formation. Precambrian Res. 200–203, 184–208. https://doi.org/10.1016/j.precamres.2012.01.018.
Sun, W.-H., Zhou, M.-F., Gao, J.-F., Yang, Y.-H., Zhao, X.-F., Zhao, J.-H., 2009. Detrital zircon U-Pb geochronological and Lu–Hf isotopic constraints on the Precambrian magmatic and crustal evolution of the western Yangtze Block, SW China. Precambrian Res. 172, 99–126. https://doi.org/10.1016/j.precamres.2009.03.010.
Tang, Q.Y., Li, C.S., Zhang, M.J., Ripley, E.M., Wang, Q.L., 2014. Detrital zircon constraint on the timing of amalgamation between Alxa and Ordos, with exploration implications for Jinchuan-type Ni–Cu ore deposit in China. Precambrian Res. 255, 748–755.
Tera, F., Wasserburg, G.J., 1972. U-Th-Pb systematics in three Apollo 14 basalts and the problem of initial Pb in lunar rocks. Earth Planet. Sci. 14, 281–304. https://doi.org/10.1016/0012-821x(72)90128-8.
Tian, R.S., Xie, G.A., Zhang, J., Zhu, W.B., Qu, J.F., Gao, S., 2019. Sedimentary provenance and age of the Langshan Group in the northeastern Alxa Block: implications for Neoproterozoic tectonic evolution. Int. J. Earth Sci. 108, 1705–1723. https://doi.org/10.1007/s00531-019-01731-9.
Tung, K.A., Yang, H.Y., Liu, D.Y., Zhang, J.X., Tseng, C.Y., Wan, Y.S., 2007a. SHRIMP U-Pb geochronology of the detrital zircons from the Longshoushan Group and its tectonic significance. Chin. Sci. Bull. 52, 1414–1425.
Tung, K.A., Yang, H.-J., Yang, H.-Y., Liu, D.Y., Zhang, J.X., Wan, Y.S., Tseng, C.-Y., 2007b. SHRIMP U-Pb geochronology of the zircons from the Precambrian basement of the Qilian Block and its geological significances. Chin. Sci. Bull. 52, 2687–2701. https://doi.org/10.1007/s11434-007-0356-0.
Turner, C.C., Meert, J.G., Pandit, M.K., Kamenov, G.D., 2014. A detrital zircon U-Pb and Hf isotopic transect across the Son Valley sector of the Vindhyan Basin, India: Implications for basin evolution and paleogeography. Gondwana Res. 26, 348–364. https://doi.org/10.1016/j.gr.2013.07.009.
Vermeesch, P., 2018. IsoplotR: a free and open toolbox for geochronology. Geosci. Front. 9, 1479–1493.
Vermeesch, P., 2021. Maximum depositional age estimation revisited. Geosci. Front. 12, 843–850. https://doi.org/10.1016/j.gsf.2020.08.008.
Wang, L.-J., Griffin, W.L., Yu, J.-H., O'Reilly, S.Y., 2013. U-Pb and Lu–Hf isotopes in detrital zircon from Neoproterozoic sedimentary rocks in the northern Yangtze Block: Implications for Precambrian crustal evolution. Gondwana Res. 23, 1261–1272. https://doi.org/10.1016/j.gr.2012.04.013.
Wang, W., Zhou, M.-F., 2012. Sedimentary records of the Yangtze Block (South China) and their correlation with equivalent Neoproterozoic sequences on adjacent continents. Sed. Geol. 265–266, 126–142. https://doi.org/10.1016/j.sedgeo.2012.04.003.
Wang, W., Chen, F.K., Hu, R., Chu, Y., Yang, Y.-Z., 2012. Provenance and tectonic setting of Neoproterozoic sedimentary sequences in the South China Block: evidence from detrital zircon ages and Hf–Nd isotopes. Int. J. Earth Sci. 101, 1723–1744. https://doi.org/10.1007/s00531-011-0746-z.
Wang, X.-L., Zhou, J.-C., Griffin, W.L., Zhao, G., Yu, J.-H., Qiu, J.-S., Zhang, Y.-J., Xing, G.-F., 2014. Geochemical zonation across a Neoproterozoic orogenic belt: Isotopic evidence from granitoids and metasedimentary rocks of the Jiangnan orogeny, China. Precambrian Res. 242, 154–171. https://doi.org/10.1016/j.precamres.2013.12.023.
Wiedenbeck, M., Allé, P., Corfu, F., Griffin, W.L., Meier, M., Oberli, F., Von Quadt, A., Roddick, J.C., Spiegel, W., 1995. Three natural zircon standards for U-TH-PB, LU-HF, trace element and ree analyses. Geostand. Geoanal. Res. 19 (1), 1–23. https://doi.org/10.1111/j.1751-908X.1995.tb00147.x.
Williams, I.S., Compston, W., Black, L.P., Ireland, T.R., Foster, J.J., 1984. Unsupported radiogenic Pb in zircon: a cause of anomalously high Pb-Pb, U-Pb and Th-Pb ages. Contrib. Mineral. Petrol. 88, 322–327. https://doi.org/10.1007/bf00376756.
Wu, S.J., Hu, J.M., Ren, M.H., Gong, W.B., Liu, Y., Yan, J.Y., 2014. Petrography and zircon U-Pb isotopic study of the Bayanwulashan Complex: Constrains on the Paleoproterozoic evolution of the Alxa Block, westernmost North China Craton. J. Asian Earth Sci. 94, 226–239. https://doi.org/10.1016/j.jseaes.2014.05.011.
Wu, C., Zuza, A.V., Yin, A., Chen, X.H., Haproff, P.J., Li, J., Li, B., Ding, L., 2021. Punctuated orogeny during the assembly of Asia: Tectonostratigraphic evolution of the North China Craton and the Qilian Shan from the Paleoproterozoic to early Paleozoic. e2020TC006503 Tectonics 40. https://doi.org/10.1029/2020tc006503.

Wu, C., Li, L., Zuza, A.V., Haproff, P.J., Yin, A., Dong, L., 2022. Paleoproterozoic-Paleozoic tectonic evolution of the Longshou Shan, western North China craton. Geosphere 18, 1177–1193. https://doi.org/10.1130/GES02491.1.

Wu, F.-Y., Yang, Y.-H., Xie, L.-W., Yang, J.-H., Xu, P., 2006. Hf isotopic compositions of the standard zircons and baddeleyites used in U-Pb geochronology. Chem. Geol. 234, 105–126.

Wu, F.-Y., Li, X.-H., Zheng, Y.-F., Gao, S., 2007. Lu-Hf isotopic systematics and their applications in petrology. Acta Petrol. Sin. 23 (2), 185–220 in Chinese with English abstract.

Xiao, Z.B., Kang, J.L., Wang, H.C., Gao, Z.R., Xiang, Z.Q., Chu, H., Ren, Y.Q., 2015. Formation age of alxa Group-complex (Special) in Alxa Area, Inner Mongolia. Geol. Surv. Res. 38 (3), 182–191 in Chinese with English abstract.

Xiao, W.Z., Lai, J.Q., Dick, J.M., Mao, X.C., Chen, Y., Ou, Q., Xie, F.Q., Zeng, R.Y., 2019. Tectonic affinity and evolution of the Alxa Block during the Neoproterozoic: Constraints from zircon U-Pb dating, trace elements, and Hf isotopic composition. Geol. J. 54, 3700–3719. https://doi.org/10.1002/gj.3343.

Xiu, Q.Y., Lu, S.N., Yu, H.F., Yang, C.L., 2002. The isotopic age evidence for main Longshoushan Group contributing to Paleoproterozoic. Prog. Precambrian Res. 25, 93–96 in Chinese with English abstract.

Xiu, Q.Y., Yu, H.F., Li, Q., Zuo, G.C., Li, J.W., Cao, C.J., 2004. Discussion on the petrogenic time of Longshoushan Group, Gansu Province. Acta Geol. Sin. 78, 366–373 in Chinese with English abstract.

Xu, X., Song, S.G., Allen, M.B., Ernst, R.E., Niu, Y.L., Su, L., 2016. An 850–820Ma LIP dismembered during breakup of the Rodinia supercontinent and destroyed by Early Paleozoic continental subduction in the northern Tibetan Plateau, NW China. Precambrian Res. 282, 52–73. https://doi.org/10.1016/j.precamres.2016.07.007.

Yan, Z., Aitchison, J., Fu, C.L., Guo, X.Q., Niu, M.L., Xia, W.J., Li, J.L., 2015b. Hualong Complex, South Qilian terrane: U-Pb and Lu–Hf constraints on Neoproterozoic micro-continental fragments accreted to the northern Proto-Tethyan margin. Precambrian Res. 266, 65–85. https://doi.org/10.1016/j.precamres.2015.05.001.

Yan, H.Q., Liu, Q.F., Tang, Z.L., Fan, M.C., Wang, Q., Ren, J.M., Fan, C.F., 2015a. Structural properties of the Longshoushan Block: Constraint from LA-ICP-MS zircon U-Pb dating (in Chinese with English abstract). Eng. Sci. 17 (2), 59–72. https://doi.org/10.3969/j.issn.1009-1742.2015.02.008.

Yang, G., Du, A.D., Lu, J.R., Qu, W.J., Chen, J.F., 2005. Re–Os dating of massive sulfide ores of the Jinchuan Ni–Cu deposit by ICP-MS. Sci. China(D) 35, 241–245 in Chinese with English abstract.

Yang, K.F., Fan, H.R., Hu, F.F., Wang, K.Y., 2012b. Sediment source of Bayan Obo marginal rift and genesis of ore-bearing dolomite of the giant REE deposit. Acta Geol. Sin. 86, 775–784 in Chinese with English abstract.

Yang, S.H., Qu, W.J., Tian, Y.L., Chen, J.F., Yang, G., Du, A.D., 2008. Origin of the inconsistent apparent Re–Os ages of the Jinchuan Ni–Cu sulfide ore deposit, China: post-segregation diffusion of Os. Chem. Geol. 247, 401–418. https://doi.org/10.1016/j.chemgeo.2007.11.002.

Yang, Q.Y., Santosh, M., Collins, A.S., Teng, X.M., 2016. Mircoblock amalgamation in the North China Craton: Evidence from Neoarchean magmatic suit in the western margin of the Jiaoliao Block. Gondwana Res. 31, 96–123.

Yang, D.-B., Xu, W.-L., Xu, Y.-G., Wang, Q.-H., Pei, F.-P., Wang, F., 2012a. U-Pb ages and Hf isotope data from detrital zircons in the Neoproterozoic sandstones of northern Jiangsu and southern Liaoning Provinces, China: Implications for the Late Precambrian evolution of the southeastern North China Craton. Precambrian Res. 216–219, 162–176. https://doi.org/10.1016/j.precamres.2012.07.002.

Yao, J.L., Cawood, P.A., Shu, L.S., Zhao, G.C., 2019. Jiangnan Orogen, South China: A ~970–820 Ma Rodinia margin accretionary belt. Earth Sci. Rev. 196, 102872 https://doi.org/10.1016/j.earscirev.2019.05.016.

Yu, J.-H., O'Reilly, S.Y., Zhou, M.-F., Griffin, W.L., Wang, L.J., 2012. U-Pb geochronology and Hf–Nd isotopic geochemistry of the Badu Complex, Southeastern China: Implications for the Precambrian crustal evolution and paleogeography of the Cathaysia Block. Precambrian Res. 222–223, 424–449. https://doi.org/10.1016/j.precamres.2011.07.014.

Yuan, W., Yang, Z.Y., 2015a. The Alashan Terrane did not amalgamate with North China block by the Late Permian: evidence from Carboniferous and Permian paleomagnetic results. J. Asian Earth Sci. 104, 145–159.

Yuan, W., Yang, Z.Y., 2015b. The Alashan Terrane was not part of North China by the Late Devonian: Evidence from detrital zircon U-Pb geochronology and Hf isotopes. Gondwana Res. 27, 1270–1282.

Zeng, R.Y., Lai, J.Q., Mao, X.C., Li, B., Zhang, J.D., Bayless, R., Yang, L.Z., 2018. Paleoproterozoic multiple tectonothermal events in the Longshoushan area, western North China Craton and their geological implication: evidence from geochemistry, zircon U-Pb geochronology and Hf Isotopes. Minerals 8, 361.

Zhai, M.G., Santosh, M., 2011. The early Precambrian odyssey of North China Craton: a synoptic overview. Gondwana Res. 20, 6–25.

Zhai, M.G., Shao, J.A., Hao, J., Peng, P., 2003. Geological Signature and Possible Position of the North China Block in the Supercontinent Rodinia. Gondwana Res. 6, 171–183. https://doi.org/10.1016/s1342-937x(05)70968-0.

Zhang, J.X., Gong, J.H., Yu, S.Y., Li, H.K., Hou, K.J., 2013b. Neoarchean-Paleoproterozoic multiple tectonothermal events in the western Alxa block, North China Craton and their geological implication: Evidence from zircon U-Pb ages and Hf isotopic composition. Precambr. Res. 235, 36–57.

Zhang, J.X., Gong, J.H., 2018. Revisiting the nature and affinity of the Alxa Block. Acta Petrol. Sin. 34 (4), 940–962 in Chinese with English abstract.

Zhang, S.-B., He, Q., Zheng, Y.-F., 2015c. Geochronological and geochemical evidence for the nature of the Dongling Complex in South China. Precambrian Res. 256, 17–30. https://doi.org/10.1016/j.precamres.2014.10.013.

Zhang, M.J., Kamo, S.L., Li, C.S., Hu, P.E., Ripley, E.M., 2010. Precise U-Pb zirconbaddeleyite age of the Jinchuan sulfide ore-bearing ultramafic intrusion, Western China. Miner Deposita 45, 3–9.

Zhang, J., Li, J.Y., Liu, J.F., Feng, Q.W., 2011. Detrital zircon U-Pb ages of Middle Ordovician flysch sandstones in the western Ordos margin: new constraints on their provenances, and tectonic implications. J. Asian Earth Sci. 42, 1030–1047.

Zhang, S.H., Li, Z.-X., Evans, D.A.D., Wu, H.C., Li, H.Y., Dong, J., 2012. Pre-Rodinia supercontinent Nuna shaping up: A global synthesis with new paleomagnetic results from North China. Earth Planet. Sci. 353–354, 145–155. https://doi.org/10.1016/j.epsl.2012.07.034.

Zhang, J., Li, J.Y., Xiao, W.X., Wang, Y.N., Qi, W.H., 2013a. Kinematics and geochronology of multistage ductile deformation along the eastern Alxa Block, NW China: new constraints on the relationship between the North China Plate and the Alxa block. J. Struct. Geol. 57, 38–57.

Zhang, W., Pease, V., Meng, Q.P., Zheng, R.G., Thomsen, T.B., Wohlgemuth-Ueberwasser, C., Wu, T.R., 2016c. Discovery of a Neoproterozoic granite in the Northern Alxa region, NW China: its age, petrogenesis and tectonic significance. Geol. Mag. 153, 512–523.

Zhang, J.J., Wang, T., Zhang, L., Tong, Y., Zhang, Z.C., Shi, X.J., Guo, L., Huang, H., Yang, Q.D., Huang, W., Zhao, J.X., Ye, K., Hou, J.Y., 2015b. Tracking deep crust by zircon xenocrysts within igneous rocks from the northern Alxa, China: Constraints on the southern boundary of the Central Asian Orogenic Belt. J. Asian Earth Sci. 108, 150–169.

Zhang, C.-L., Ye, X.-T., Zou, H.-B., Chen, X.-Y., 2016a. Neoproterozoic sedimentary basin evolution in southwestern Tarim, NW China: New evidence from field observations, detrital zircon U-Pb ages and Hf isotope compositions. Precambrian Res. 280, 31–45. https://doi.org/10.1016/j.precamres.2016.04.011.

Zhang, J., Zhang, Y.P., Xiao, W.X., Wang, Y.N., Zhang, B.H., 2015a. Linking the Alxa Terrane to the eastern Gondwana during the Early Paleozoic: Constraints from detrital zircon U-Pb ages and Cambrian sedimentary records. Gondwana Res. 28, 1168–1182.

Zhang, J., Zhang, B.H., Zhao, H., 2016b. Timing of amalgamation of the Alxa Block and the North China Block: Constraints based on detrital zircon U-Pb ages and sedimentologic and structural evidence. Tectonophysics 668–669, 65–81.

Zhao, G.C., 2009. Metamorphic evolution of major tectonic units in the basement of the North China Craton: key issues and discussion. Acta Petrol. Sin. 25, 1772–1792 in Chinese with English abstract.

Zhao, G.C., Cawood, P.A., 2012. Precambrian geology of China. Precambrian Res. 222–223, 13–54. https://doi.org/10.1016/j.precamres.2012.09.016.

Zhao, J.-H., Li, Q.-W., Liu, H., Wang, W., 2018b. Neoproterozoic magmatism in the western and northern margins of the Yangtze Block (South China) controlled by slab subduction and subduction-transform-edge-propagator. Earth Sci. Rev. 187, 1–18. https://doi.org/10.1016/j.earscirev.2018.10.004.

Zhao, G.C., Wilde, S.A., Cawood, P.A., Sun, M., 2001. Archean blocks and their boundaries in the North China Craton: lithological, geochemical, structural and P-T path constrains and tectonic evolution. Precambrian Res. 107, 45–73.

Zhao, G.C., Cawood, P.A., Wilde, S.A., Sun, M., 2002. Review of global 2.1-1.8 Ga orogens: Implications for a pre-Rodinia supercontinent. Earth Sci. Rev. 59, 125–162.

Zhao, G.C., Sun, M., Wilde, S.A., Li, S.Z., 2005. Late Archean to Paleoproterozoic evolution of the North China Craton: key issues revisited. Precambrian Res. 136, 177–202.

Zhao, G.C., Wilde, S.A., Guo, J.H., Cawood, P.A., Sun, M., Li, X.P., 2010b. Single zircon grains record two Paleoproterozoic collisional events in the North China Craton. Precambrian Res. 177, 266–276.

Zhao, G.C., Wang, Y.J., Huang, B.C., Dong, Y.P., Li, S.Z., Zhang, G.W., Yu, S., 2018a. Geological reconstructions of the East Asian blocks: From the breakup of Rodinia to the assembly of Pangea. Earth Sci. Rev. 186, 262–286. https://doi.org/10.1016/j.earscirev.2018.10.003.

Zhao, X.-F., Zhou, M.-F., Li, J.-W., Sun, M., Gao, J.-F., Sun, W.-H., Yang, J.-H., 2010a. Late Paleoproterozoic to early Mesoproterozoic Dongchuan Group in Yunnan, SW China: Implications for tectonic evolution of the Yangtze Block. Precambrian Res. 182, 57–69. https://doi.org/10.1016/j.precamres.2010.06.021.

Zheng, R.G., Wu, T.R., Zhang, W., Xu, C., Meng, Q.P., Zhang, Z.Y., 2014. Late Paleozoic subduction system in the northern margin of the Alxa block, Altaids: geochronological and geochemical evidences from ophiolites. Gondwana Res. 25, 842–858.

Zheng, R.G., Li, Y.J., Xiao, W.J., Wang, L.J., 2018. A new ophiolitic mélange containing boninitic blocks in Alxa region: Implications for Permian subduction events in southern CAOB. Geosci. Frontiers 9, 1355–1367.

Zhong, Y., Zhai, M., Peng, P., Santosh, M., Ma, X., 2015. Detrital zircon U-Pb dating and whole-rock geochemistry from the clastic rocks in the northern marginal basin of the North China Craton: Constraints on depositional age and provenance of the Bayan Obo Group. Precambrian Res. 258, 133–145. https://doi.org/10.1016/j.precamres.2014.12.010.

Zhou, Z., Hu, M., Wu, C., Wang, G., Liu, C., Cai, A., Jiang, T., 2017. Coupled U-Pb dating and Hf isotopic analysis of detrital zircons from Bayan Obo Group in Inner Mongolia: Constraints on the evolution of the Bayan Obo rift belt. Geol. J. 53, 2649–2664. https://doi.org/10.1002/gj.3102.